CrossMark

J. Fluid Mech. (2017), *vol.* 813, *pp.* 824–859. © Cambridge University Press 2017
doi:10.1017/jfm.2016.818

On reduced models for gravity waves generated by moving bodies

Philippe H. Trinh†

Oxford Centre for Industrial and Applied Mathematics, Mathematical Institute, University of Oxford, Oxford OX2 6GG, UK

(Received 7 December 2015; revised 25 November 2016; accepted 30 November 2016; first published online 26 January 2017)

In 1983, Tulin published a report proposing a framework for reducing the equations for gravity waves generated by moving bodies into a single nonlinear differential equation solvable in closed form (*Proceedings of the 14th Symposium on Naval Hydrodynamics*, 1983, pp. 19–51). Several new and puzzling issues were highlighted by Tulin, notably the existence of weak and strong wave-making regimes, and the paradoxical fact that the theory seemed to be applicable to flows at low speeds, 'but not too low speeds'. These important issues were left unanswered, and despite the novelty of the ideas, Tulin's report fell into relative obscurity. Now, 30 years later, we will revive Tulin's observations, and explain how an asymptotically consistent framework allows us to address these concerns. Most notably, we demonstrate, using the asymptotic method of steepest descents, how the production of free-surface waves can be related to the arrangement of integration contours connected to the shape of the moving body. This approach provides a new and powerful methodology for the study of geometrically nonlinear wave–body interactions.

Key words: surface gravity waves, waves/free-surface flows, wave–structure interactions

1. Introduction

The motivation for this paper stems from an important, but seemingly forgotten 1983 report by Professor Tulin presented during the 14th Symposium on Naval Hydrodynamics, titled 'An exact theory of gravity wave generation by moving bodies, its approximation and its implications' (Tulin 1983). Some 30 years after its publication, Tulin wrote of his original motivation for pursuing the former study:

> What were the relations and connections among these various nonlinear approximations – ray, 'slow ship', second order, formal straining, and Guilloton – that had arisen by the end of the 1970s? [· · ·] I had earlier in the 1970s become intrigued by the Davies transformation of the nonlinear free-surface problem, which was revealed in Milne–Thompson's legendary banquet speech (in 1956). So I set out to extend it from its previous application for progressive waves, to include the presence of a submerged wave-making body. My hope was that my extension of the

† Email address for correspondence: trinh@maths.ox.ac.uk

https://doi.org/10.1017/jfm.2016.818 Published online by Cambridge University Press

> Davies theory would provide an exact result in analytical form, which even in its complexity could then be subject to various approximations, the connections of which could thereby be discerned. And so it turned out. (Tulin 2005, p. 242)

In the 1983 paper, Tulin sought to derive a rigorous mathematical reduction of the water-wave equations in such a way that certain nonlinear contributions within the free-surface equations could be preserved. The resultant model was analytically simple, and took the form of a single complex-valued linear differential equation given by (cf. § 2.1)

$$\left\{\frac{\epsilon}{G}\frac{\mathrm{d}G}{\mathrm{d}w} - \frac{\mathrm{i}}{G} + \mathcal{P}(w, q, \theta)\right\} = -\mathcal{Q}(w), \tag{1.1}$$

where $G = (q\mathrm{e}^{-\mathrm{i}\theta})^3$ is a nonlinear function of the fluid speed, q, and streamline angle θ. The independent variable, w, is the complex potential, $\mathcal{P}$ is a nonlinear function of the unknowns, and $\mathcal{Q}$ is a function that encodes the details of the wave-generating body. The non-dimensional parameter

$$\epsilon = F^2 = \frac{U^2}{gL} \tag{1.2}$$

is the square of the Froude number for upstream speed U, gravity g, and length scale L.

The theory surrounding (1.1) is powerful, as it provides a formulation relating the geometry of a moving body directly with the resultant free-surface waves. However, several important and surprising issues were raised by Tulin regarding the model and its interpretation, and in particular, he had noted a paradoxical behaviour present at low speeds, $\epsilon \to 0$. In the years that followed, perhaps owing to the difficulty of the model's derivation, Tulin's fundamental questions were never readdressed. In this paper, we shall present an asymptotically consistent derivation that corrects Tulin's model, and puts to rest many of the issues previously highlighted.

In addition, we will connect Tulin's investigations to a separate line of research by Tuck (1990, 1991*a*,*b*) who, within a series of papers, had attempted to distil the wave-making properties of wave–body problems into a linear singular equation. The model Tuck proposed was (cf. § 2.2)

$$\epsilon^2\frac{\mathrm{d}^2y}{\mathrm{d}\phi^2} + y = \mathcal{F}(\phi), \tag{1.3}$$

where now y is the free-surface height, ϕ the velocity potential, and $\mathcal{F}$ serves a similar purpose to Tulin's $\mathcal{Q}$ function and thus describes the geometry of the solid body. Although Tuck's reduced framework was only meant to be pedagogical and illustrative, it exhibits some deeper aspects of wave–structure theory which we shall elucidate. A historical overview of the two reduced models will follow in § 2.

1.1. *Goals of this paper*

We have three principal goals in this work.

(i) We wish to demonstrate how Tulin's formulation (1.1) can be systematically derived and studied in the low-speed limit. The source of Tulin's puzzling results can be resolved through better understanding of two effects: first, the *ad hoc* linearization

https://doi.org/10.1017/jfm.2016.818 Published online by Cambridge University Press

of the nonlinear $\mathcal{P}$ function; and second, the role of the forcing function, $\mathcal{Q}$. We clarify these details and demonstrate the numerical convergence of the different proposed models in the limit $\epsilon \to 0$.

One of our principal results (presented on page 16) is to demonstrate that the water waves, valid as $\epsilon \to 0$, are described to leading order by solutions, $\bar{q}$, of the complex-valued equation,

$$\epsilon \bar{q}' + \left[\frac{\mathrm{i}j}{q_0^3} + \epsilon \left(\frac{2q_0'}{q_0} - \frac{3\mathrm{i}jq_1}{q_0^4} \right) \right] \bar{q} = R(w; \hat{\mathscr{H}}[\bar{\theta}]), \tag{1.4}$$

where $j = \pm 1$ is a parameter related to the physical geometry. The observable real-valued physical waves, q_{exp}, are then given by the sum of $\bar{q}$ and its complex conjugate. Different choices of the right-hand side of (1.4) only change the predicted wave amplitudes by a numerical factor. The leading order $\epsilon \to 0$ solution, q_0, contains the prescription of the moving body, and can thus be related to Tuck's $\mathcal{F}$ function in (2.6). The formulation in terms of the speed, q, rather than Tulin's combined function $G = (q\mathrm{e}^{-\mathrm{i}\theta})^3$ in (1.1) is more natural, but we will relate Tulin's equation to our own in § 6 and appendix C.

(ii) We also study the associated integral form of the solution using the method of steepest descents. We shall demonstrate how the appearance of surface waves can be associated with sudden deformations of the integration contour when a solution to (1.4) is analytically continued across critical curves (Stokes lines) in the complex plane. This process is known as the Stokes phenomenon (Berry 1991; Olde Daalhuis *et al.* 1995; Trinh 2010).

(iii) Our last goal is to provide a link between the Tulin formulation (1.1), Tuck formulation (1.3), our corrected model, and also the current research on low-Froude-number approximations.

2. A historical overview of nonlinear wave–body models

2.1. *Tulin's water-wave model*

The essential derivation behind Tulin's model begins from Bernoulli's equation applied to a free surface with streamline, $\psi = 0$,

$$\frac{\epsilon}{q} \frac{\mathrm{d}q}{\mathrm{d}\phi} + \frac{\sin\theta}{q^3} = 0, \tag{2.1}$$

where q is the fluid speed, θ the streamline angle, ϕ the potential, ϵ is given by (1.2). If the sinusoidal term is split according to the identity

$$3\sin\theta = \sin 3\theta + 4\sin^3\theta, \tag{2.2}$$

then (2.1) can be written in complex-valued form as

$$\mathrm{Re}\left\{ \frac{\epsilon}{G} \frac{\mathrm{d}G}{\mathrm{d}w} - \frac{\mathrm{i}}{G} + \mathcal{P}(w, q, \theta) \right\} = 0, \tag{2.3}$$

where $G = (q\mathrm{e}^{-\mathrm{i}\theta})^3$ is an analytic function of the complex potential, $w = \phi + \mathrm{i}\psi$, and the above is evaluated on $\psi = 0$ where $\mathrm{Re}(\mathcal{P}) = 4\sin^3\theta/q^3$.

The rather curious substitution of (2.2) is attributed to Davies (1951, p. 478), who had argued that if $\mathcal{P}$ is considered to be small, then (2.3) yields a linearized version

https://doi.org/10.1017/jfm.2016.818 Published online by Cambridge University Press

of Bernoulli's equation (in G) that preserves the essential nonlinearity (in q^3), which describes the structure of a steep gravity wave with a crest angle near 120°. As explained by Davies, the rationale is that the nonlinear variation in the speed of a sharp-crested wave is an essential component to preserve, but not so much the variation in θ.

Inspired by this idea, Tulin considered the extension to general free-surface flows over a moving body. Since the function in the curly braces of (2.3) is an analytic function in w, except at isolated points in the complex plane, then analytic continuation implies

$$\left\{\frac{\epsilon}{G}\frac{\mathrm{d}G}{\mathrm{d}w} - \frac{\mathrm{i}}{G} + \mathcal{P}(w, q, \theta)\right\} = -\mathcal{Q}(w), \tag{2.4}$$

where by matching to uniform flow, $G \to 1$ and thus $\mathcal{Q} \to \mathrm{i}$ in the upstream limit. The function $\mathcal{Q}(w)$ is purely imaginary on $\psi = 0$. In the case of flow without a body or bottom boundary, $\mathcal{Q} \equiv \mathrm{i}$, but otherwise, $\mathcal{Q}$ will encode the effect of the obstructions through its singular behaviour in the complex plane. If the nonlinear contribution, $\mathcal{P}$, is neglected in (1.1), then the solution can be written as

$$G(w) = \left[\frac{\mathrm{i}}{\epsilon}\int^{w} \mathrm{e}^{\frac{1}{\epsilon}\int^{t}\mathcal{Q}(s)\,\mathrm{d}s}\,\mathrm{d}t\right]\mathrm{e}^{-\frac{1}{\epsilon}\int^{w}\mathcal{Q}(s)\,\mathrm{d}s}, \tag{2.5}$$

where the lower limit of integration should be chosen to zero the constant of integration. Hence (2.5) yields Tulin's exact theory.

This process seems to yield the exponentially small surface waves at low speeds. However, Tulin noted that as $\epsilon \to 0$, there would be locations on the free surface where $\mathcal{Q} = 0$, and this would lead to unbounded steepness. He wrote of

> ... the revelation that for sufficiently strong disturbances ... waves arise at discrete points on the free surface which ... do not become exponentially small with decreasing Froude number, but rather tend to unbounded steepness as $F \to 0$.

He thus proposed the following result:

> The most important comment to make is that for given ϵ, no matter how small, this so-called low-speed theory is not valid for sufficiently low speeds. It is a theory valid for low, but not too low speeds!

The matter was left at that, and in the three decades following Tulin's ingenious paper, the peculiarities surrounding the asymptotic breakdown of (1.1) were never directly readdressed (although we mention the paper by Vanden-Broeck & Miloh (1995) which develops numerical solutions for the case $\mathcal{Q} = \text{const.}$ and $\mathcal{P} \neq 0$).

Note that in addition to the investigation in the limit $\epsilon \to 0$, Tulin had also intended to produce an exact reduction, where the $\mathcal{P}$ term in (1.1) was handled through a theoretically posited nonlinear coordinate transformation. However, it is never clear how this transformation is used or derived in practice, except through nonlinear computation of the full solutions.

https://doi.org/10.1017/jfm.2016.818 Published online by Cambridge University Press

2.2. *Tuck's linearized integral equation*

Independently from Tulin, Tuck later presented a series of papers (Tuck 1990, 1991*a*,*b*) where he attempted to distil the wave-making properties of wave–body problems into a linear singular equation. The equation presented (equation (22) of Tuck (1991*a*)) was

$$\epsilon \mathscr{H} \frac{\mathrm{d}y}{\mathrm{d}\phi} + y = \mathcal{F}(\phi), \tag{2.6}$$

where $y(\phi)$ is the height of the free surface, $\mathcal{F}(\phi)$ is a function related to the moving body, and $\mathscr{H}$ is an integral operator known as the Hilbert transform (to be introduced in § 3). The difficulty in solving (2.6) is that the Hilbert transform is a global operator, requiring values of y over the entire domain.

In the 1991*a* work, Tuck explained how the action of $\mathscr{H}$ could be viewed as similar to that of the differential operator $\mathrm{d}/\mathrm{d}\phi$. This reduction was mostly pedagogic in nature, but Tuck was motivated by the fact that $\mathscr{H}$ and the differential operator will act similarly in the case of sinusoidal functions. By replacing $\mathscr{H}$ by $\epsilon\mathrm{d}/\mathrm{d}\phi$, he went on to study the various properties of the singular differential equation

$$\epsilon^2 \frac{\mathrm{d}^2 y}{\mathrm{d}\phi^2} + y = \mathcal{F}(\phi), \tag{2.7}$$

that depend on the specification of the 'body' given by $\mathcal{F}(\phi)$.

Apparently, Tuck had been unaware of Tulin's (1983) work, but a chance meeting of the two occurred during a conference leading to the publication of Tuck (1991*b*). We are fortunate enough to possess the archived questions of the meeting, where we discover that Tulin had asked the following question:

> Isn't it true that the two dimensional wavemaker problem can be presented in terms of an ordinary differential equation in the complex domain, at least to some higher order of approximation? (Tuck 1991*b*, p. 237)

Tuck replied that he was unsure of the generality of the reduction to problems including different geometries, but noted the connection to the Davies (1951) reduction (2.2):

> I do not know the answer to this question ... My '$[\mathcal{F}(x)]$' in some way represents a very general family of 'wavemakers', with structure in both spatial dimensions, and I have doubts as to whether the problem can then be converted (exactly) to a differential equation. On the other hand, a few years ago I in fact used the method that you describe, and it is associated with the approximation $\sin\theta \approx \frac{1}{3}\sin 3\theta$.

Although Tuck's toy reduction (1.3) should only be regarded as illustrative (the governing differential equation should rather be first order), what is apparent in his work is the desire to systematically reduce both the nonlinearity of Bernoulli's equation, and the global effect of $\mathscr{H}$ into a single ordinary differential equation. In particular, it is Tuck's search for a reduction of the operator, $\mathscr{H}$, that was missing from earlier works on this topic (including Tulin 1983).

https://doi.org/10.1017/jfm.2016.818 Published online by Cambridge University Press

2.3. *Other works and reductions*

Certainly, Tulin and Tuck were not the only ones to seek simpler reductions or formulations of the nonlinear equations for wave–body interactions, and indeed, Tulin relates his work to the integral models proposed by Dawson (1977) and Inui & Kajitani (1977). Reviews of these and other models were presented by Doctors & Dagan (1980) and Miloh & Dagan (1985), and many others. However, what distinguishes Tulin and Tuck's work is the shifted focus towards the analytic continuation of the flow problem into the complex domain.

As we have noted in § 2.1, the low-Froude-number or low-speed limit of $\epsilon \to 0$ is the essential approximation in which analytical results can be derived. The subtleties of studying this singular limit can be traced back to a seminal report by Ogilvie (1968). Ogilvie explained the importance of this regime, but then detailed certain oddities with the previously developed analytical approximations of free-surface flow past a submerged body. Chief amongst such oddities was the fact that the individual terms of a series approximation in powers of ϵ would fail to predict surface waves. Thus, one might decompose the surface speed into a regular series expansion and an error term, $\bar{q}$, with

$$q(\phi) \sim [q_0(\phi) + \epsilon q_1(\phi) + \cdots + \epsilon^{N-1} q_{N-1}(\phi)] + \bar{q}(\phi). \tag{2.8}$$

The challenge, Ogilvie realized, was that water waves are exponentially small in ϵ, with $\bar{q} = O(\mathrm{e}^{-const./\epsilon})$, and thus beyond all orders of any individual term of the regular series.

By linearizing about the zeroth-order solution, $q = q_0 + \bar{q}$ for $\bar{q} \ll 1$, and strategically preserving certain terms in Bernoulli's equation, Ogilvie developed a general analytical approximation for the exponentially small surface waves. The approximation, however, was not asymptotically consistent, and the search for a complete numerical and analytical treatment of the low-Froude-number limit would inspire many papers in the subsequent years.

One of the key issues we will explore in this paper addresses the question of how many terms must be included in the linearization of (2.8) in order to obtain the exponential. Originally Ogilvie (1968) had chosen $N = 1$, but later revised to $N = 2$ in Ogilvie & Chen (1982) (who quoted the work of Dagan & Tulin (1972) and in particular, the study by Keller (1979) in applying the WKB method to streamline ship waves).

We shall not pursue, in great detail, the history of the low-Froude-number problem that followed Ogilvie's seminal report, but instead refer to the review papers by Tuck (1991*a*) and, particularly, Tulin (2005) where certain aspects of the low-Froude-number difficulty are discussed. Additional historical details are presented in § 1 of Trinh, Chapman & Vanden-Broeck (2011), and a selection of papers on the problem is presented in table 1. The method we apply in this paper, which combines an approach of series truncation with the method of steepest descents, is unique from the previously listed works.

Note furthermore that the low-Froude-number steady-flow regime studied in this paper only forms one piece of the very large puzzle of free-surface wave–structure interactions (albeit a significant one in the context of nonlinear geometries). In other regimes, such as for the case of supercritical flows ($\epsilon > 1$), it may be possible to derive further analytical insights (cf. Craig & Sternberg 1992; Tulin 2005; Vanden-Broeck 2010). However, the connection between different regimes remains a non-trivial problem for future research; we shall return to discuss the inclusion of additional effects in § 10.

https://doi.org/10.1017/jfm.2016.818 Published online by Cambridge University Press

Historical significance	Papers
Origin of the low-Froude-number paradox	Ogilvie (1968)
Two-dimensional and three-dimensional linearizations	Dagan & Tulin (1972), Keller (1979), Doctors & Dagan (1980), Ogilvie & Chen (1982), Tulin (1984), Brandsma & Hermans (1985)
On numerical solutions	Vanden-Broeck & Tuck (1977), Vanden-Broeck, Schwartz & Tuck (1978), Madurasinghe & Tuck (1986), Farrow & Tuck (1995)
On exponential asymptotics applied to water waves	Chapman & Vanden-Broeck (2002, 2006), Trinh *et al.* (2011), Lustri, McCue & Chapman (2013), Trinh & Chapman (2013*a*,*b*), Lustri & Chapman (2014), Trinh & Chapman (2014)
Review articles	Tuck (1991*a*), Tulin (2005)

TABLE 1. The development of the low-Froude-number paradox.

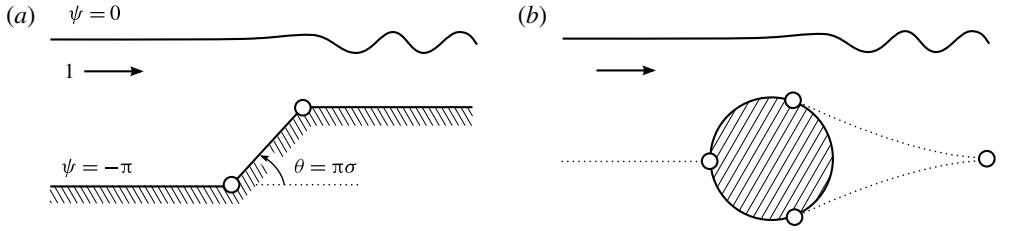


FIGURE 1. (*a*) Non-dimensional flow over an angled step in a channel and (*b*) flow past a circular cylinder. The dimensionalization is discussed in § 3.1. Flows past closed bluff objects can be complicated through wake separation (seen *b*), for which the nature of the separation points is unclear.

3. Mathematical formulation

Let us consider steady irrotational two-dimensional flow past a moving body in the presence of gravity, g. The body is associated with a length scale L, and moves at constant velocity U. For instance, this body may correspond to an obstacle at the bottom of the channel (figure 1*a*), a submerged object (figure 1*b*) or a surface-piercing ship (figure 2*a*). We shall state more precise geometrical restrictions in § 3.1.

The velocity potential, ϕ, satisfies Laplace's equation in the fluid region, $\nabla^2\phi = 0$. On all boundaries, the kinematic condition implies the normal derivative is zero, $\partial\phi/\partial n = 0$, while on the free surface, Bernoulli's equation requires that

$$\tfrac{1}{2}(|\nabla\phi|^2 - U^2) + gy = \text{const.} \tag{3.1}$$

Subsequently, all quantities are non-dimensionalized using the velocity and lengths scales, U and L, and we introduce a Cartesian coordinate system (x, y) such that the body is fixed in the moving frame of reference.

With $z = x + \mathrm{i}y$, we define the complex potential, $w = \phi + \mathrm{i}\psi$, and the complex velocity is given by,

$$\frac{\mathrm{d}w}{\mathrm{d}z} = q\mathrm{e}^{-\mathrm{i}\theta}. \tag{3.2}$$

https://doi.org/10.1017/jfm.2016.818 Published online by Cambridge University Press

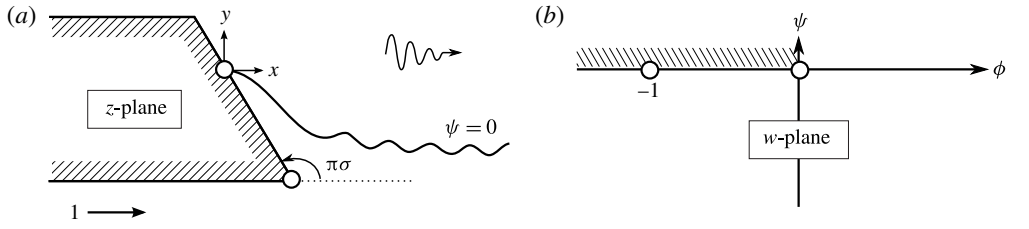


FIGURE 2. (*a*) Physical z-plane and (*b*) potential w-plane for stern flow past a one-cornered ship.

Here ψ is the streamfunction, q is the fluid speed and θ is the streamline angle, measured from the positive x-axis. Without loss of generality, we choose $\psi = 0$ on the free surface and $\psi < 0$ within the fluid. We define the logarithmic hodograph variable,

$$\Omega = \log q - \mathrm{i}\theta, \tag{3.3}$$

and seek to solve the flow problem inversely, that is, use w as an independent variable and seek $\Omega = \Omega(w)$ in the lower-half w-plane. The advantage of this hodograph formulation is that with the free surface at $\psi = 0$, its position is known in the (ϕ, ψ)-plane, even though its shape in the physical (x, y)-plane is unknown. Differentiating Bernoulli's equation with respect to ϕ and using (3.2) then yields the non-dimensionalized form (2.1).

3.1. *Boundary integral formulation and geometrical examples*

In theory, the methods we present in this paper will apply to most general two-dimensional free-surface flows. In practice, however, in order to make analytical progress, we will be constrained by problems in which the geometry of the body is known through the specification of the angle, θ, in terms of the complex potential, $w = \phi + \mathrm{i}\psi$.

As specific examples, let us focus on two representative geometries: (*a*) flow past a localized obstruction on a channel bottom (figure 1*a*) and (*b*) flow past a semi-infinite surface piercing ship (figure 2*a*).

For flow past a varying channel bottom with dimensional upstream depth h, we select the length scale $L = h/\pi$, so that the flow region in the w-plane consists of an infinite strip between $0 \leqslant \psi \leqslant \pi$. The strip is then mapped to the upper-half ζ-plane, using

$$\zeta = \xi + \mathrm{i}\eta = \mathrm{e}^{-w}, \tag{3.4}$$

where under (3.4), the free surface is mapped to $\xi \geqslant 0$, the channel bottom to $\xi \leqslant 0$, and the flow region to $\eta \geqslant 0$.

For flows past a semi-infinite surface piercing body, we can choose the length scale to be $L = K/U$, where K is a representative scale of the potential along the body (see (2.3) in Trinh & Chapman (2014) for further details). We assume that the free surface attaches to the body at a stagnation point, chosen without loss of generality to be $\phi = 0$. In the potential plane, the flow region consists of $\psi \leqslant 0$. On the boundary $\psi = 0$, $\phi > 0$ corresponds to the free surface and $\phi < 0$ to the solid body. Since the flow is already contained within a half-plane, we do not need a further $w \mapsto \zeta$ transformation, as in (3.4), but we shall set $\zeta = w$ so as to use the same notation.

https://doi.org/10.1017/jfm.2016.818 Published online by Cambridge University Press

Bernoulli's equation (2.1) provides an explicit relationship between the real and imaginary parts of Ω on the free surface. However, because Ω is analytic in the upper or lower-half ζ-plane and tends to zero far upstream, there is a further Hilbert transform relationship between its real and imaginary parts. Applying Cauchy's theorem to Ω over a large semi-circle in the upper (channel flow) or lower (surface-piercing flow) half-ζ-planes, and taking the real part gives the principal value integral,

$$\log q = \frac{j}{\pi} \fint_{-\infty}^{\infty} \frac{\theta(\xi')}{\xi' - \xi} \, \mathrm{d}\xi' \quad \text{for } \xi \in \mathbb{R}, \tag{3.5}$$

where $j = -1$ for flow in the channel configuration and $j = 1$ for flow in the ship configuration. The range of integration can be split into an evaluation over the solid boundary and over the free surface. We write

$$\log q = \log q_s + j\mathscr{H}[\theta](\xi) \quad \text{for } \xi \in \mathbb{R}, \tag{3.6}$$

where $\mathscr{H}$ denotes the Hilbert transform operator on the semi-infinite interval,

$$\mathscr{H}[\theta](\xi) = \frac{1}{\pi} \fint_{0}^{\infty} \frac{\theta(\xi')}{\xi' - \xi} \, \mathrm{d}\xi'. \tag{3.7}$$

We assume that for a given physical problem, the angle θ is known for the particular geometry, and thus the function q_s that appears in (3.6) is known through calculating

$$\log q_s = \frac{j}{\pi} \int_{-\infty}^{0} \frac{\theta(\xi')}{\xi' - \xi} \, \mathrm{d}\xi'. \tag{3.8}$$

Note that it is somewhat misleading to describe $\theta(\xi)$ as 'known' for $\xi < 0$ since in practice, we would specify θ as a function of the physical coordinates (x, y). However, specifying different forms of θ as a function of ξ (or the potential, ϕ) is typically sufficient to obtain the qualitatively desired geometry shape. Once the values of q and θ are known on the free surface, their values everywhere within the fluid can be computed using Cauchy's theorem. Consequently, the flow in the physical (x, y)-plane can be retrieved by integrating (3.2).

For instance, we consider the step geometry,

$$\theta_{step} = \begin{cases} 0 & \xi \in (-\infty, -b) \cup (-a, 0) \\ \pi\sigma & \xi \in (-b, -a), \end{cases} \tag{3.9}$$

where $0 < a < b$, which corresponds to a step of angle $\pi\sigma$. Such topographies have been considered by King & Bloor (1987), Chapman & Vanden-Broeck (2006), Lustri, McCue & Binder (2012), others. In this case, (3.4), (3.8) and (3.9) yields

$$q_s = \left(\frac{\xi + b}{\xi + a}\right)^{\sigma} = \left(\frac{\mathrm{e}^{-\phi} + b}{\mathrm{e}^{-\phi} + a}\right)^{\sigma}. \tag{3.10}$$

Similarly, a semi-infinite ship with a single corner of angle $\pi\sigma$ can be specified using

$$\theta_{ship} = \begin{cases} 0 & \phi \in (-\infty, -1) \\ \pi\sigma & \phi \in (-1, 0). \end{cases} \tag{3.11}$$

Such two-dimensional hull shapes have been considered in the works of Vanden-Broeck *et al.* (1978), Farrow & Tuck (1995), Trinh *et al.* (2011), and others. Choosing

https://doi.org/10.1017/jfm.2016.818 Published online by Cambridge University Press

the dimensional length, $L = K/U$ where K is the value of the potential at the corner sets its non-dimensional position to $\phi = -1$. Then using (3.8) and (3.11), the q_s function is given by

$$q_s = \left(\frac{\xi}{\xi+1}\right)^{\sigma} = \left(\frac{\phi}{\phi+1}\right)^{\sigma}. \tag{3.12}$$

Recall the ship problem does not require an additional mapping to the half plane, so we can set $\zeta = w$ to preserve the notation.

In this paper, we will only consider geometries which contain strong singularities in the complex plane; these correspond to poles or branch points in q_s. For instance, the step (3.10) and ship (3.12) contain singularities at the corners and stagnation points of the body. We will see in § 8 that these singularities are often responsible for the creation of the surface waves. Weaker singularities, such as the case of flow past a smoothed hull with a jump in the curvature, will be the subject of a forthcoming paper (cf. also § 7 of Trinh & Chapman 2014). Flows past closed objects also present challenging cases for study because typically the geometry is not known as a function of the potential variables, and there are further difficulties with the prediction of wake separation points (figure 1*b*).

The situation of steady-state gravity waves requires specification of additional radiation or boundary conditions. In the case of step flow in a channel, we impose a uniform flow upstream,

$$q \to 1, \quad \theta \to 0 \quad \text{as } \phi \to -\infty. \tag{3.13a,b}$$

For the case of stern flow past a ship, we require that the flow separates at a stagnation point, and the necessary conditions on q and θ were derived by Dagan & Tulin (1972). If it is the case that $\sigma \geqslant 1/3$, then the flow separates horizontally from the body and this requires that

$$q = O(\phi^{\sigma}), \quad \theta = O(\phi^{3\sigma-1}) \quad \text{as } \phi \to 0. \tag{3.13c,d}$$

If $\sigma < 1/3$, then the flow separates so as to make an interior angle of $2\pi/3$ with the body. Steady-state bow flows are typically not possible unless the free surface is allowed to form a splash. Further extended discussions of the requisite boundary conditions are found in Vanden-Broeck (2010), Trinh *et al.* (2011), and the references therein.

Thus the governing equations consist of Bernoulli's equation (2.1), the boundary integral equation (3.6), a specified geometry, and the radiation or boundary conditions (3.13).

4. The failure of the typical asymptotic expansion

In this section, we demonstrate that the regular expansion of the solution of Bernoulli's equation (2.1) and the boundary integral (3.6) is divergent, and moreover fails to capture the free-surface waves.

In the limit $\epsilon \to 0$, we substitute a regular asymptotic expansion, $q = q_0 + \epsilon q_1 + O(\epsilon^2)$ and $\theta = \theta_0 + \epsilon\theta_1 + O(\epsilon^2)$ into the two governing equations, and obtain for the first two orders,

$$q_0 = q_s, \qquad \theta_0 = 0, \tag{4.1a,b}$$

$$q_1 = jq_0\mathscr{H}[\theta_1], \quad \theta_1 = -q_0^2\frac{\mathrm{d}q_0}{\mathrm{d}\phi}. \tag{4.1c,d}$$

https://doi.org/10.1017/jfm.2016.818 Published online by Cambridge University Press

Thus, at leading order, the free surface is entirely flat, $\theta_0 = 0$, and this solution is known as the rigid wall solution. The leading-order speed, $q_0 = q_s$, is given by (3.10) for the step, or (3.12) for the ship, but fails to capture the surface waves. Because all the subsequent orders in the asymptotic scheme depend on derivatives of the leading-order solution, it stands to reason that it is impossible to encounter a sinusoidal term, despite going to any algebraic order in ϵ.

Using the numerical algorithms outlined Trinh *et al.* (2011), we calculate the solutions of (2.1) and (3.6) for the case of a rectangular ship, with $\sigma = 1/2$ and $\epsilon = 1.0$. This is shown in figure 3.

4.1. *Divergence of the asymptotic approximation*

The leading-order approximation, q_0, contains singularities in its analytic continuation into the complex plane. For instance, in the case of the step geometry (3.10), we see that q_0 contains branch points at $\xi = -a$ and $\xi = -b$, which correspond to the corner and stagnation points.

Because of the singularly perturbed nature of Bernoulli's equation in the limit $\epsilon \to 0$, we can see that at each order in the asymptotic procedure, the calculation of q_n and θ_n will depend on differentiation of the previous order, q_{n-1} and θ_{n-1}. Since the leading-order approximation is singular, this has the effect of increasing the power of the singularities with each subsequent term. Thus in the limit that $n \to \infty$, q_n and θ_n will diverge. As argued in the works of e.g. Chapman, King & Adams (1998), Chapman & Vanden-Broeck (2006), the divergence at $O(\epsilon^n)$ is captured through a factorial over power ansatz,

$$q_n \sim \frac{Q\Gamma(n+\gamma)}{\chi^{n+\gamma}} \quad \text{and} \quad \theta_n \sim \frac{\Theta\Gamma(n+\gamma)}{\chi^{n+\gamma}}, \tag{4.2a,b}$$

where $\chi = 0$ at the particular singularity. The functions Q, Θ, and χ may be regarded as either functions of w or of ζ. If there are multiple singularities contributing to the divergence (see Trinh & Chapman (2014) for an example), then we must include a summation over similar ansatzes of the form (4.2) where $\chi = 0$ at each individual singularity. There exist other cases where a more general form of the divergence is required, and this is documented in Trinh & Chapman (2015).

In order to derive the components, Q, χ, and γ, we can examine the $O(\epsilon^n)$ form of the system, and take the limit $n \to \infty$. In this paper, the late-orders behaviour is not a crucial part of the analysis, but we collect the functional forms of the components in appendix A.

5. Analytic continuation of the governing equations

In §§ 7 and 8, we will demonstrate that the leading-order water waves can be described by an integral equation, which is then approximated by deforming the path of integration into the complex plane. Thus, it will be necessary for us to study the analytic continuation (or complexification) of the free-surface quantities. Below, we explain this for the $\zeta = \xi + \mathrm{i}\eta$-plane defined in § 3.1, but the same ideas apply for continuation directly in the $w = \phi + \mathrm{i}\psi$-plane.

(i) Firstly, we note that on the free surface, where $\eta = 0$ and $\xi > 0$, the two quantities $q(\xi)$ and $\theta(\xi)$ are real-valued analytic functions of ξ. We seek to analytically continue q and θ from the free surface into the upper and lower half ξ-planes; this results in two new complex-valued analytic functions,q_c, $\theta_c : \mathbb{C} \to \mathbb{C}$,

https://doi.org/10.1017/jfm.2016.818 Published online by Cambridge University Press

https://doi.org/10.1017/jfm.2016.818 Published online by Cambridge University Press

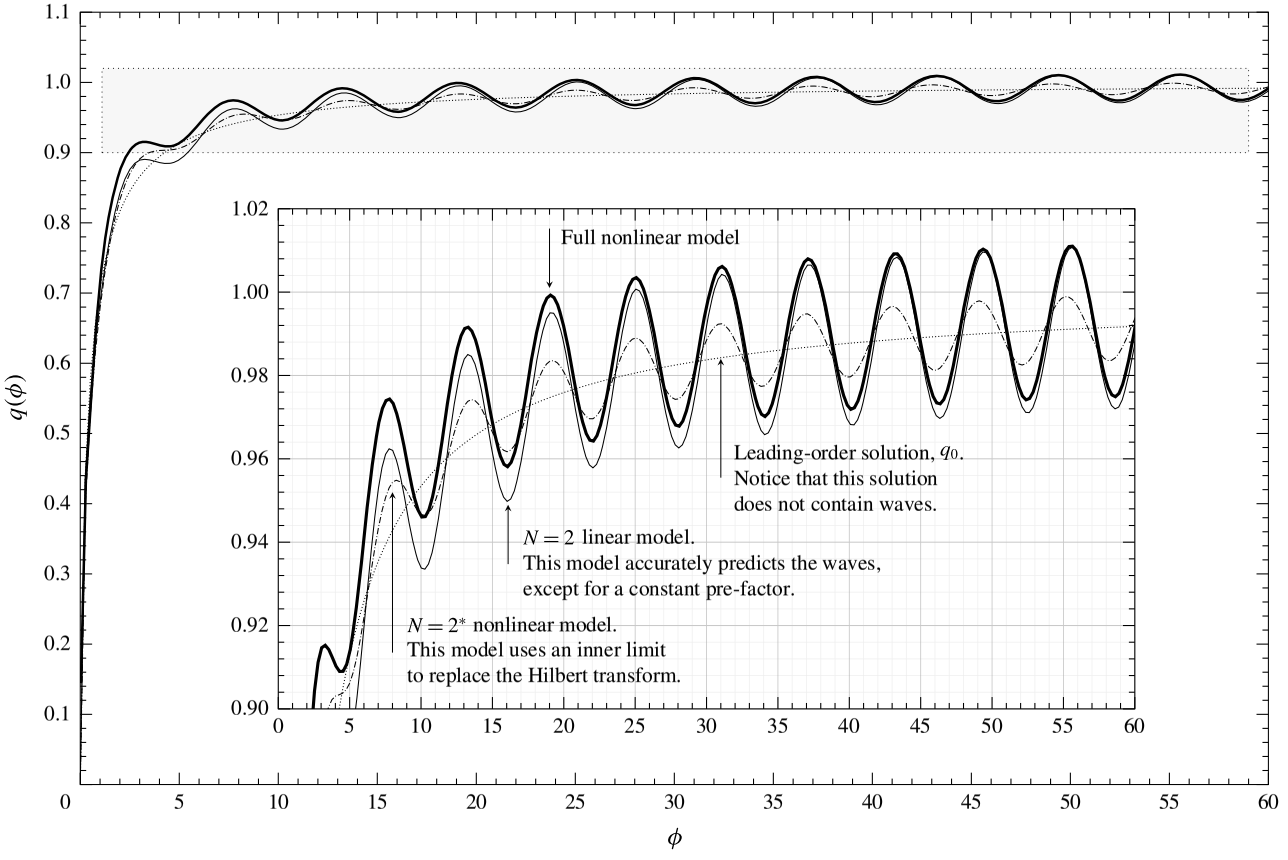


FIGURE 3. Numerical solution (thick line) of the full stern-flow problem (2.1), (3.6), and (3.13*c*,*d*) with $\epsilon = 1.0$ and $\sigma = 1/2$. The dotted line is the leading-order approximation q_0. Also shown are the solutions, $q_0 + 2\mathrm{Re}(\bar{q})$, from the truncated linear $N = 2$ model (thin line) and the truncated nonlinear $N = 2^*$ model (dash-dotted line). These models are discussed in § 9 and summarized in table 2.

such that for $\xi > 0$,

$$q_c(\xi \pm \mathrm{i}0) = q(\xi) \quad \text{and} \quad \theta_c(\xi \pm \mathrm{i}0) = \theta(\xi). \tag{5.1a,b}$$

(ii) From the above properties, at every point $\xi > 0$, both q and θ can be expanded into a Taylor series in powers of ξ with real coefficients. Evaluation of the series for complex ξ is one fashion to obtain q_c and θ_c, but the convergence of the series will be limited by singularities in the complex plane. Instead, complexified versions of Bernoulli's equation (2.1) and the boundary integral (3.6) are used for the analytic continuation process.

Bernoulli's equation (2.1) is extended in a straightforward manner and only requires that the independent variable in the differential equation, ϕ, be treated as complex valued. The result is stated below in (5.6*a*).

Thus we set $\xi \mapsto \xi_r + \mathrm{i}\xi_i$ and discuss the complexification of the boundary integral (3.6). For analytic continuation into the upper half-plane, we can verify that in the limit $\xi_i \to 0$ from the upper half-plane,

$$\frac{1}{\pi}\int_0^\infty \frac{\theta(\xi')}{\xi' - (\xi_r + \mathrm{i}\xi_i)}\ \mathrm{d}\xi' = \frac{1}{\pi}\!\!\int_0^\infty \frac{\theta(\xi')}{\xi' - \xi_r}\ \mathrm{d}\xi' + \frac{1}{\pi}\int \frac{\theta(\xi')}{\xi' - \xi_r}\ \mathrm{d}\xi', \tag{5.2}$$

where the second integral on the right-hand side corresponds to the counterclockwise integral around $\xi' = \xi$ along a small semi-circle. An analogous argument applies for continuation into the lower half-plane. Relabelling $\xi = \xi_r + \mathrm{i}\xi_i = \zeta$, we have that the analytic continuation of the Hilbert transform, $\mathscr{H}$, is given by

$$\mathscr{H}[\theta](\zeta) = \hat{\mathscr{H}}[\theta](\zeta) - \mathrm{i}k\theta_c(\zeta), \tag{5.3}$$

where $k = 1$ for analytic continuation into the upper half-ζ-plane, $k = -1$ for the continuation into the lower half-plane, and we have introduced the notation $\hat{\mathscr{H}}$ for the integral on the left-hand side of (5.2),

$$\hat{\mathscr{H}}[\theta](\zeta) = \frac{1}{\pi}\int_0^\infty \frac{\theta(\xi')}{\xi' - \zeta}\ \mathrm{d}\xi'. \tag{5.4}$$

Note that the Hilbert transforms, $\mathscr{H}$ and $\hat{\mathscr{H}}$, always operate on θ along the free surface, rather than the analytically continued function, θ_c.

Thus the analytic continuation of the boundary integral equation (3.6) is given by

$$\log q_c + (jk)\mathrm{i}\theta_c = \log q_s + j\hat{\mathscr{H}}[\theta]. \tag{5.5}$$

(iii) In the bulk of this paper, we focus on the analytic continuation into the upper half-ζ-plane and thus set $k = 1$ in (5.5). Since it follows that q_c and θ_c are real on the axis, their values in the lower half-plane follows from Schwarz's reflection principle (later this is applied specifically in § 8.4). Note that following (5.2), we had relabelled the new complex variable $\xi \mapsto \zeta$. We shall do the same for the extension of the real potential $\phi \mapsto w$. Moreover, we drop the subscripted notation of q_c and θ_c.

Then the two analytically continued governing equations, valid in the upper half-plane, are given by

$$\epsilon q^2 \frac{\mathrm{d}q}{\mathrm{d}w} + \sin\theta = 0, \tag{5.6a}$$

$$\log q + \mathrm{i}j\theta = \log q_s + j\hat{\mathscr{H}}[\theta]. \tag{5.6b}$$

https://doi.org/10.1017/jfm.2016.818 Published online by Cambridge University Press

It is possible to combine the two equations into a single complex-valued integro-differential equation. We write the sine term of (5.6*a*) in terms of complex exponentials using (5.6*b*), giving

$$\sin\theta = \frac{1}{2\mathrm{i}}\left[\left(\frac{q_s}{q}\right)^j \mathrm{e}^{\hat{\mathscr{H}}[\theta]} - \left(\frac{q}{q_s}\right)^j \mathrm{e}^{-\hat{\mathscr{H}}[\theta]}\right]. \tag{5.7}$$

We then simplify (5.7) using $j=\pm 1$, and substitute into Bernoulli's equation (5.6*a*) to obtain the following combined integro-differential formulation.

GOVERNING EQUATIONS. *[Analytic continuation of water waves] We seek to study the analytically continued equations for the speed, q, and angle θ, off the free surface and into the upper half-ζ-plane. The combined integro-differential formulation is*

$$\epsilon\frac{\mathrm{d}q}{\mathrm{d}w} + \frac{\mathrm{i}j}{2}\frac{1}{q_s q^3}[q^2 e^{-j\hat{\mathscr{H}}[\theta]} - q_s^2 e^{j\hat{\mathscr{H}}[\theta]}] = 0, \tag{5.8}$$

which forms two equations (real and imaginary parts) for the two unknowns q and θ. In (5.8), q_s contains the problem geometry as defined by (3.10) and (3.12), the analytically continued Hilbert transform, $\hat{\mathscr{H}}$, is defined in (5.3), and we have defined the constant

$$j = \begin{cases} 1 & \text{for surface-piercing flow,} \\ -1 & \text{for channel flow.} \end{cases} \tag{5.9}$$

For the channel geometry, we use the conformal map from the potential strip to the ζ-plane given by $\zeta = e^{-w}$, while for the surface-piercing geometry, $\zeta = w$.

In all subsequent formulae, we will sometimes use ζ and w interchangeably in the functional notation, e.g. writing $q = q(w)$ or $q = q(\zeta)$ depending on the particular context. In general, primes ($'$) will be used solely for differentiation in w.

5.1. *Further notes on the analytic continuation process*

There are subtle aspects of analytically continuing q and θ off the free surface, and the relationship of these quantities with the usual physical complex velocity given by $\mathrm{d}w/\mathrm{d}z = u - \mathrm{i}v = q\mathrm{e}^{-\mathrm{i}\theta}$. The q_c and θ_c that appear on the left-hand side of (5.5) are complex valued, but reduce to the physical speed and velocities on the free surface, $\zeta = \xi > 0$. Although their combined values, $q_c\mathrm{e}^{-\mathrm{i}\theta_c}$, are related to the complex velocity, $u - \mathrm{i}v$, their individual values are not known without further work.

As an example of this particular subtlety, we may consider the analytic continuation of θ, evaluated along the physical boundary, $\zeta \leqslant 0$. In general, this value, θ_c, will not be the physical angle as defined in (3.9) or (3.11). Instead, the analytic continuations of the individual components, q_c and θ_c, are related to the physical angle through $\mathrm{Im}[\log(q_c\mathrm{e}^{-\mathrm{i}\theta_c})]$.

In this work, we will depend on asymptotic derivations of the analytic continuation variables, q_c and θ_c. However, it is also possible to numerically solve the nonlinear equations (5.6) for such quantities; this is done for the study of travelling waves of permanent form in Crew & Trinh (2016).

https://doi.org/10.1017/jfm.2016.818 Published online by Cambridge University Press

6. Connections to Tulin's formulation

The reader will notice that we have somewhat strayed from our original motivation of studying Tulin's formulation presented in § 2.1, where the governing equations are posed in terms of a combined analytic quantity, $G(w)$, in (1.1). Tulin's formulation can be adjusted to use the substitution $G = (q\mathrm{e}^{-\mathrm{i}j\theta})^3$, where $j = \pm 1$ as in (5.9). This modifies the analytically continued Bernoulli's equation to

$$\frac{\epsilon}{G}\frac{\mathrm{d}G}{\mathrm{d}w} - \frac{\mathrm{i}j}{G} + \mathcal{P}(w, q, \theta) = -\mathcal{Q}(w), \tag{6.1}$$

for function, $\mathcal{P}$ with $\mathrm{Re}(\mathcal{P}) = 4\sin^3\theta/q^3$, which had resulted from the sine reduction (2.2), and for some $\mathcal{Q}$ that has yet to be specified. The adjustment of including $j = \pm 1$ serves to orient the fluid with respect to the solid boundary, and facilitates comparison with our (5.8).

We highlight two main differences between our (5.8) and Tulin's formulation (6.1). First, in ours, we have chosen to work with analytic continuations of q and θ independently, whereas Tulin has combined $G = (q\mathrm{e}^{-\mathrm{i}j\theta})^3$, so as to advantageously write the left-hand side of (6.1) in an elegant form. However, the nonlinear term, $\mathcal{P}$, cannot be easily written as a function of G, and this nonlinear term will be important in the analysis to come. It is unclear whether it is possible to provide a complete formulation without independently treating q and θ, as we have done in our (5.8).

The second main difference is that (5.8) is self-contained and thus readily solved numerically or asymptotically, whereas the $\mathcal{Q}$-function in (1.1) is unknown. Like the introduction of G, while the introduction of the $\mathcal{Q}$-function is elegant in appearance, its connection to the low-Froude-number asymptotics is difficult to elucidate.

We have included a discussion of Tulin's original interpretation of the $\mathcal{Q}$-function in appendix B. To summarize the conclusions of the discussion: the $\mathcal{Q}$-function can be written as a boundary integral evaluated over the solid boundary and its reflected image in the potential or ζ-plane. However, this resultant quantity cannot be known without first solving the free-surface problem (2.1) and (3.6). Thus, $\mathcal{Q}$ should rather be written

$$\mathcal{Q}(w) = \mathcal{Q}(w, q(w), \theta(w)), \tag{6.2}$$

and it becomes difficult to unravel components of $\mathcal{Q}$ that are crucial to the determination of the free-surface waves. Our formulation (5.8) sidesteps this by explicitly including the local and global aspects of the problem in form that can be computed numerically and asymptotically. Once we have understood how (5.8) is reduced in the $\epsilon \to 0$, it will be possible to demonstrate more clearly how Tulin's formulation relates. We will do this in appendix C.

7. Reduction to a simplified model

The study of the nonlinear integro-differential equation (5.8) is primarily complicated because of the non-local nature of the Hilbert transform $\hat{\mathscr{H}}$. In § 2.2, we had reviewed the efforts of E.O. Tuck, who attempted to convert $\hat{\mathscr{H}}$ into a local operator. In this section and the next, we shall demonstrate that, while the Hilbert transform is crucial for determining the corrections to the rigid-body solution (cf. the dotted curve in figure 3), the waves can be derived largely independently from $\hat{\mathscr{H}}$.

We first introduce the truncated regular expansion

$$q_r = \sum_{n=0}^{N-1} \epsilon^n q_n \quad \text{and} \quad \theta_r = \sum_{n=0}^{N-1} \epsilon^n \theta_n, \tag{7.1a,b}$$

https://doi.org/10.1017/jfm.2016.818 Published online by Cambridge University Press

where q_r and θ_r are seen to be waveless, that is to say, they do not possess any oscillatory component. The oscillatory components will be introduced via a linearization of the solution about the regular expansion. We set,

$$q = q_r + \bar{q} \quad \text{and} \quad \theta = \theta_r + \bar{\theta}, \tag{7.1c,d}$$

where we assume $\bar{q}, \bar{\theta} = o(\epsilon^{N-1})$.

Our strategy is to substitute (7.1) into the integro-differential equation (5.8), and then separate the terms proportional to $\bar{q}$ onto the left-hand side. Simplification then leads to the main result of this paper.

PRINCIPAL RESULT 1 (REDUCED INTEGRO-DIFFERENTIAL MODEL). *Linearizing the water-wave equations about a regular series expansion truncated at N terms gives the following integro-differential equation for the perturbation,*

$$\epsilon\bar{q}' + \left[\chi'(w) + \epsilon P_1'(w) + O(\epsilon^2)\right]\bar{q} = R(w; \hat{\mathscr{H}}[\bar{\theta}]) + O(\bar{\theta}^2, \bar{q}^2), \tag{7.2a}$$

where

$$\chi'(w) = \frac{\mathrm{i}j}{q_0^3(w)}, \tag{7.2b}$$

$$P_1'(w) = \left(2\frac{q_0'}{q_0} - 3\mathrm{i}j\frac{q_1}{q_0^4}\right), \tag{7.2c}$$

$$R(w; \hat{\mathscr{H}}[\bar{\theta}]) = [-\mathcal{E}_{bern} - \mathrm{i}j\mathcal{E}_{int}]\frac{\cos\theta_r}{q_r^2} + \mathrm{i}\hat{\mathscr{H}}[\bar{\theta}]\frac{\cos\theta_r}{q_r^2}, \tag{7.2d}$$

and q_0 and q_1 are given in (4.1a,b) and (4.1c,d). The error term, $\mathcal{E}_{bern}$, represents the error in Bernoulli's equation, and is given by

$$\mathcal{E}_{bern} = \epsilon q_r' + \frac{\sin\theta_r}{q_r^2}, \tag{7.2e}$$

while the error term, $\mathcal{E}_{int}$, in the integral equation is given by

$$\mathcal{E}_{int} = \log q_r + \mathrm{i}j\theta_r - (\log q_0 + j\hat{\mathscr{H}}[\theta_r]). \tag{7.2f}$$

The function χ that appears in (7.2*b*) is the same as the singulant function that describes the factorial-over-power divergence (4.2) and whose value is found in appendix A through the study of the regular asymptotic expansion of the solutions. Similarly, in the next section, P_1 will be related to Q, which appears in (4.2).

We will use the notation of $R(w)$ and $R(w; \hat{\mathscr{H}}[\bar{\theta}])$ interchangeably, preferring the latter when we wish to emphasize that R depends on the inclusion of the Hilbert transform. Notice also that the system (7.2) will undergo significant changes in its written form as soon as $w = \phi + \mathrm{i}\psi$ or $\zeta = \xi + \mathrm{i}\eta$ approaches the free surface (either $w \in \mathbb{R}$ or $\zeta \in \mathbb{R}^+$). When this occurs, the integral $\hat{\mathscr{H}}[\bar{\theta}]$ must be written as a principal value and residue contribution, as in (5.2). In other words, though it is written in a complex-valued form, (7.2) will necessarily reduce to a real-valued equation along the free surface.

https://doi.org/10.1017/jfm.2016.818 Published online by Cambridge University Press

7.1. *Truncation and optimal truncation*

The crucial decision in studying the system (7.2) is to choose how many terms to include in the truncated series, q_r and θ_r, which determines the forcing function R. That is, we must choose the truncation value of N.

In early studies of the low-Froude-number problem, researchers had used $N=1$, and then later corrected to $N=2$. However, at a fixed value of ϵ, the truncation error in the divergent asymptotic expansion will continue to decrease for increasing values of N. It reaches a minimum at an optimal truncation point, $N=\mathcal{N}$, and diverges afterwards. For small ϵ, the optimal truncation point is found where adjacent terms in the series are approximately equal in size, or $|\epsilon^{\mathcal{N}} q_{\mathcal{N}}| \sim |\epsilon^{\mathcal{N}-1} q_{\mathcal{N}-1}|$. Using the divergent form (4.2), we find that the optimal truncation point is given by

$$\mathcal{N} \sim \frac{|\chi(w)|}{\epsilon}. \tag{7.3}$$

Thus, for a fixed point in the domain, w, and in the limit $\epsilon \to 0$, the optimal truncation point, $\mathcal{N}$, tends to infinity, and we must include infinitely many terms of the series. In § 9, we will examine the effect of different truncations on the comparison between numerical solutions and asymptotic approximations.

Most emphatically, we remark that apart from the hidden $O(\epsilon^2)$ terms multiplying $\bar{q}$ in the brackets of (7.2*a*), this reduced equation is an exact result to all orders in ϵ. We have only employed the fact $\bar{q}, \bar{\theta} \ll 1$, but the inhomogeneous term, $R(w)$ is exact. When the regular series expansions are optimally truncated, $\bar{q}$ and $\bar{\theta}$ are exponentially small, and consequently, the $O(\bar{q}^2, \bar{\theta}^2)$ terms are not needed to derive the leading-order behaviour of the exponentials.

Though it is now written as a first-order differential equation, the system (7.2) is difficult to solve, since it involves real and complex components, in addition to the integral transforms embedded in the inhomogeneous term. The key in the following sections will be to argue that the Hilbert transform can be neglected.

8. General analysis using steepest descents

The main goal in this section is to demonstrate how the reduced integro-differential equation (7.2) can be written as an explicit integral, which is then approximated using the method of steepest descents (for details of this method, see for example Bleistein & Handelsman 1975). In fact, it is this steepest descents analysis that rectifies the unanswered issues from Tulin's work.

In this paper, we will present the main ideas of a steepest descents analysis applied to the integral solution of (7.2). In practice, the individualized steepest descent paths must be studied for each different moving body (as specified by the q_s function in (3.8)). In a companion paper (Trinh 2016), the full steepest descent structure is derived for the case of flow over a step and past the stern of a ship. This latter analysis requires careful consideration of the branch structures and numerically generated contours of the integrand, so we relegate the details to the companion study.

8.1. *Integral form of the solution*

To begin, we integrate (7.2*b*) to obtain

$$\chi(w) = \mathrm{i}j \int_{w_0}^{w} \frac{\mathrm{d}\varphi}{q_0^3(\varphi)}. \tag{8.1}$$

https://doi.org/10.1017/jfm.2016.818 Published online by Cambridge University Press

In the above integral, the initial point of integration, w_0, is chosen to be the particular point that causes the divergence of the late-order terms in (4.2). Thus, χ defined in (7.2) matches the definition of the singulant function in the late-orders ansatz.

Next integrating (7.2*c*),

$$P_1(w) = -\log \Lambda + \log\left[\frac{q_0^2(w)}{q_0^2(w^*)}\right] - 3\mathrm{i}j\int_{w^*}^{w} \frac{q_1(\varphi)}{q_0^4(\varphi)}\,\mathrm{d}\varphi, \tag{8.2}$$

where $-\log\Lambda$ is the constant of integration, and w^* can be chosen wherever the integral is defined. We also note that P_1 given by (8.2) is related to Q given in (A 3). We can then write

$$\mathrm{e}^{-P_1(w)} = q_0^2(w^*)Q(w) = \left[\frac{\Lambda q_0^2(w^*)}{q_0^2(w)}\right]\exp\left(3\mathrm{i}j\int_{w^*}^{w}\frac{q_1(\varphi)}{q_0^4(\varphi)}\,\mathrm{d}\varphi\right). \tag{8.3}$$

Solving (7.2*a*) now yields a solution for the integro-differential equation (though note that it is not quite explicit due to the reliance on the Hilbert transform),

$$\bar{q}(w) = \left[\frac{Q(w)}{\epsilon}\right]\{I(w) + \text{const.}\} \times \mathrm{e}^{-\chi(w)/\epsilon}, \tag{8.4a}$$

where we have introduced the integral

$$I(w) = \int_{w_s}^{w} R(\varphi;\, \hat{\mathscr{H}}[\bar{\theta}])\left[\frac{1}{Q(\varphi)} + O(\epsilon)\right]\mathrm{e}^{\chi(\varphi)/\epsilon}\,\mathrm{d}\varphi, \tag{8.4b}$$

which will be used to extract the prefactor of the exponential. The start point, w_s, can be chosen based on additional boundary or radiation conditions. For channel flow, the water wave problem will naturally impose a radiation condition which requires the free surface to be flat at $\phi = -\infty$ (upstream), so taking $w_s \to -\infty$, the constant of integration in (8.4*a*) is zero. Similarly, for the surface-piercing problem, w_s can be taken to be the stagnation point, $w_s = 0$, where $q = 0$.

8.2. *The steepest descent paths*

For the integral (8.4*b*), the paths of steepest descent are given by constant contours of $\mathrm{Im}\,\chi$. Let us envision a generic situation in which the steepest descent topology is as shown in the figure 4(*a*). A critical point (branch point, singularity, or saddle point) of the integrand is assumed to lie at $w = w_0$. The valleys, where $\mathrm{Re}[\chi(w)] \leqslant \mathrm{Re}[\chi(w_0)]$, are shown shaded. In the illustrated case, the path of steepest descent from the initial, $t = w_s$, and final point, $t = w$, is joined by a single valley of the integrand. Thus, we write

$$I(w) \sim I_{endpoints}, \tag{8.5}$$

and the relevant contributions to the integral solely depend upon an expansion about the endpoints. When we perform this analytically in § 8.3, we find that the $I_{endpoint}$ contribution yields further algebraic orders of the base asymptotic series, q_r and θ_r. In other words, (8.5) leads to further deflections of the free surface due to the moving body, but does not produce an oscillatory component.

The oscillatory contributions arise from the deformation of the path of integration through the critical points of the integrand. A typical situation is illustrated in

https://doi.org/10.1017/jfm.2016.818 Published online by Cambridge University Press

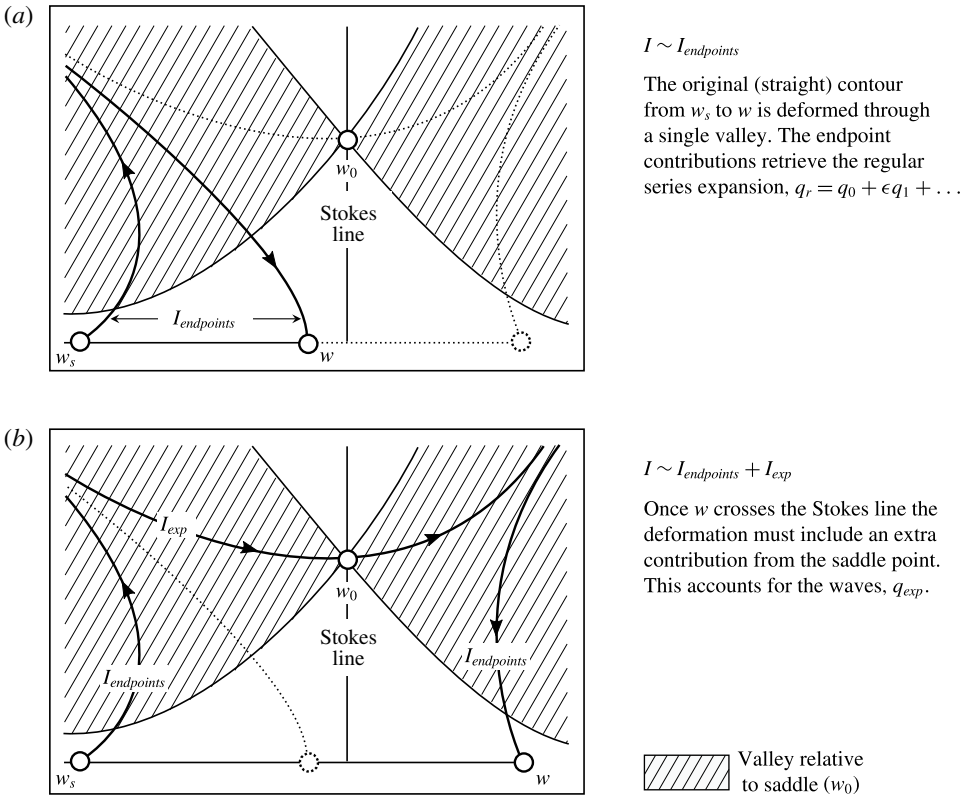


FIGURE 4. Illustration of steepest descent contours for a problem with a single wave-generating singularity, $w = w_0$. (*a*) When the endpoint of integration lies to the left of the Stokes line, $I \sim I_{endpoints}$; (*b*) when the end of integration crosses the Stokes line, the steepest descent path must include the contribution from the saddle.

figure 4(*b*). There, we see that if the endpoint, $t = w$, crosses the Stokes line, $\mathrm{Im}[\chi] = \mathrm{Im}[\chi(w_0)]$ from the point, $t = w_0$, then the steepest descent paths from each individual endpoint tend to distinct valleys. These valleys must be joined by a contour through the saddle or around the critical point. In such cases, we shall write

$$I(w) \sim I_{endpoints} + I_{exp}. \tag{8.6}$$

In this work, we do not discuss the global properties of the steepest descent curves and the associated Stokes lines. These results require careful consideration of the Riemann-sheet structure of the integrand, and can be found in the accompanying work (Trinh 2016). Instead, we assume that the integral is approximated by (8.6), and numerically verify the approximation in § 9.

8.3. *Endpoint contributions*

It can be verified that the dominant contributions from the endpoints will re-expand the regular perturbation series to higher orders. In particular, we see from inspection

https://doi.org/10.1017/jfm.2016.818 Published online by Cambridge University Press

that locally near $t = w$, the integrand is exponentially large and of order $\mathrm{e}^{\chi/\epsilon}$, and this serves to cancel the exponentially small factor in (8.4*a*).

The form of the integral in (8.4) is unwieldy, so we shall demonstrate this re-expansion for the simplest case where the regular series, q_r and θ_r, contains only a single term. Setting $q_r = q_0 = q_s$ and $\theta_r = \theta_0 = 0$ from (4.1*a*,*b*) and using (7.2*d*–*f*) the integral is reduced to

$$I_{endpoints} \sim \int_{w_s}^{w} \left[-\epsilon q_0' + \frac{\mathrm{i}\hat{\mathscr{H}}[\bar{\theta}]}{q_0^2} \right] \left[\frac{1}{Q(\varphi)} + O(\epsilon) \right] \mathrm{e}^{\chi(\varphi)/\epsilon} \, \mathrm{d}\varphi. \tag{8.7}$$

Integrating by parts, we have

$$I_{endpoints} \sim \frac{\epsilon}{\chi'} \left[-\epsilon q_0' + \frac{\mathrm{i}\hat{\mathscr{H}}[\bar{\theta}]}{q_0^2} \right] \left[\frac{1}{Q(w)} + O(\epsilon) \right] \mathrm{e}^{\chi(w)/\epsilon}, \tag{8.8}$$

where we have assumed that the boundary term contributions due to $\varphi = w_s$ are zero from the boundary or radiation conditions (see the discussion following (8.4*b*)). Repeated integration by parts to the integral term of (8.7) will extract further contributions. We keep only the first term above, and recombine with $\bar{q}$ in (8.4*a*) to obtain

$$\bar{q} \sim \frac{q_0^3}{\mathrm{i}j} \left[-\epsilon q_0' + \frac{\mathrm{i}\mathscr{H}[\bar{\theta}]}{q_0^2} - \frac{\bar{\theta}}{q_0^2} \right], \tag{8.9}$$

where we have used (5.3) and (7.2*b*). Matching real and complex parts then yields $\bar{q} = jq_0\mathscr{H}[\bar{\theta}]$ and $\bar{\theta} = -\epsilon q_0^2 q_0'$, which are the first correction terms derived in (4.1*c*,*d*). The procedure to obtain further corrections proceeds in a similar way using repeated integration by parts, and thus producing further powers of ϵ.

Including more terms from q_r and θ_r and performing the re-expansion procedure about the endpoints will follow the same idea; algebraically, however, it is much easier to work with the integro-differential equation (7.2*a*), or simply with the original system of two coupled equations, as was done in § 4.

8.4. *The Hankel contour*

In the limit $\epsilon \to 0$, the contributions to the contour integral associated with wave motion arises from cases where the contour is deformed past critical points in the integrand, or near saddle points, where $\chi' = 0$. Let us assume that the contribution occurs at a point, $w = w_0$, where $\chi'(w_0) = 0$ and that w_0 lies off the free surface (see § 10.2 for comments on other cases). Locally near this point, we assume that the leading-order speed behaves as

$$q_0 \sim c(w - w_0)^{\alpha}, \tag{8.10}$$

for some constants c and α. Consequently, it follows from (7.2*b*) that

$$\chi \sim X(w - w_0)^{1-3\alpha} \quad \text{where } X = \frac{\mathrm{i}j}{c^3(1 - 3\alpha)}. \tag{8.11}$$

One of the key issues that underlies the Tulin reduction of the water-wave equations concerns the role of the non-local Hilbert transform, $\hat{\mathscr{H}}$, which appears in the forcing

https://doi.org/10.1017/jfm.2016.818 Published online by Cambridge University Press

function $R(w;\ \hat{\mathscr{H}}[\bar{\theta}])$ in (7.2*d*). In the previous section, we discovered that the Hilbert transform plays an important role in the further development of the endpoint contributions. Indeed, it appears as a contributing term in each order of the asymptotic process, beginning from q_1 in (4.1*c*,*d*).

Upon applying the method of steepest descents to the integral I, we had separated the contributions into those due to endpoints and those due to saddle points (assumed to lie away from the free surface). Let us assume that the contribution due to the saddle point is exponentially small along the free surface, with $\bar{q}_{exp} = O(\mathrm{e}^{-\chi/\epsilon})$ in (8.4*a*), with $\mathrm{Re}(\chi) > 0$ on the free surface, and similar relations for $\bar{\theta}$. As the variable of integration approaches the saddle point, $\varphi \to w_0$, the term

$$\mathrm{i}\hat{\mathscr{H}}[\bar{\theta}]\frac{\cos\theta_r}{q_r^2} \tag{8.12}$$

that appears in R of (7.2*d*) involves the integration of an exponentially small term along the free surface, where it remains exponentially small. Thus, this term is subdominant to the square-bracketed contributions in (7.2*d*). This argument does not work for the endpoint contributions; the Hilbert transform is not negligible, as it involves the integration of the regular perturbative series via $\hat{\mathscr{H}}[\theta_r]$.

We now approximate the contribution near the saddle points. As discussed in § 7.1, as $\epsilon \to 0$, the optimal truncation point, $N \to \infty$. Thus using the divergent form (4.2), we have that

$$R \sim -\epsilon^N q'_{N-1} \sim \epsilon^N \frac{Q\Gamma(N+\gamma)\chi'}{\chi^{N+\gamma}}, \tag{8.13}$$

away from the real axis. Recall that the components, Q, γ, and χ are given in appendix A. Thus substituting (8.13) into (8.4*b*), we have

$$I_{exp} \sim \epsilon^N \Gamma(N+\gamma) \int_{C_0} \left[\frac{\chi'}{\chi^{N+\gamma}}\right] \mathrm{e}^{\chi/\epsilon}\ \mathrm{d}\varphi. \tag{8.14}$$

In (8.14), the contour C_0 corresponds to the steepest descents contour in the vicinity of the critical point, $\varphi = w_0$. Near this point, we simplify the exponential by making a coordinate transformation with

$$u = \frac{X(\varphi - w_0)^{1-3\alpha}}{\epsilon} \quad \text{and thus} \quad \chi \sim \epsilon u \tag{8.15}$$

from (8.11). It thus follows from (8.14) that

$$I_{exp} \sim \frac{\Gamma(N+\gamma)}{\epsilon^{\gamma-1}} \int_{C_0} u^{-(N+\gamma)}\mathrm{e}^u\ \mathrm{d}u. \tag{8.16}$$

Based on the steepest descent topologies corresponding to the ship and step problems, the relevant local contribution near $\varphi = w_0$ occurs in the form of a Hankel contour – that is, an integral about the branch cut $u \in \mathbb{R}^-$, beginning from $u = -\infty - 0\mathrm{i}$, looping around the origin, and tending to $u = -\infty + 0\mathrm{i}$. These steepest descent topologies are the subject of the companion paper (Trinh 2016). By the integral definition of the gamma function,

$$\oint_{C_0} u^{-(N+\gamma)}\mathrm{e}^u\ \mathrm{d}u = \frac{2\pi\mathrm{i}}{\Gamma(N+\gamma)}. \tag{8.17}$$

https://doi.org/10.1017/jfm.2016.818 Published online by Cambridge University Press

Therefore, combining with (8.16), we have $I_{exp} \sim 2\pi \mathrm{i} \epsilon^{1-\gamma}$. We may now substitute this approximation for I_{exp} into (8.4*a*) to obtain the part of $\bar{q}$ that is switched-on by the saddle point contribution. This yields

$$\bar{q}_{exp} \sim \left[\frac{2\pi \mathrm{i} Q(w)}{\epsilon^{\gamma}} \right] \mathrm{e}^{-\chi(w)/\epsilon}, \tag{8.18}$$

where $Q(w)$ is given in (8.3).

Recall that the functional form of integrand in (8.4*b*) changes in the limit the real axis is approached due to the presence of the complex Hilbert transform in R. Moreover, the derivation of (8.18) only takes in account the steepesst descent paths for analytic continuation into the upper half-ζ-plane ($k = 1$). Repeating the process for the lower half reflects the steepest descent paths about the real axis.

Rather than repeating the procedure and observing the change in signs of k, we can note that wave component of q or θ must be real along the physical free surface. Consequently, by the Schwarz reflection principle, the leading-order wave solution must be the sum of (8.18) and its complex conjugate. Thus on the free surface, where $w = \phi$,

$$q_{exp}(\phi) \sim \left[\frac{2\pi \mathrm{i} Q(\phi)}{\epsilon^{\gamma}} \right] \mathrm{e}^{-\chi(\phi)/\epsilon} + \text{c.c.} \tag{8.19}$$

In numerical computations, it is typically easiest to compare the wave amplitudes in the far field, where $w = \phi \to \infty$, and the mean speed, $q_r \to 1$. For simplicity we choose the integral limit w^* in Q to be on the free surface. Substituting (8.3) into (8.19) and simplifying gives the amplitude of the oscillations,

$$\text{Amplitude of waves in } q \sim \frac{4\pi |\Lambda|}{\epsilon^{\gamma}} \mathrm{e}^{-\mathrm{Re}(\chi)/\epsilon}, \quad \text{as } \phi \to \infty, \tag{8.20}$$

where the constant Λ appears in the expression for Q and its value must be computed numerically for general nonlinear problems (see appendix A). In the end, (8.20) provides a closed-form formula for the amplitude of the waves, which only depends on specification of the two solutions, q_0 and q_1, calculated from (4.1), and late-order components, Λ, γ, and χ, given in appendix A. Note that q_1 is needed to calculate the value of Λ.

Finally, we can establish an equation between the exponentially small waves in q and θ. Upon substituting (7.1) into (5.6*b*), we have that

$$\theta_{exp} = \left[\frac{-\mathrm{i} j}{q_0} + O(\epsilon) \right] q_{exp}. \tag{8.21}$$

9. Comparisons of the full nonlinear model with the reduced models

In the last two sections, we derived a reduced model for the wave–body interaction, and subsequently explained how asymptotic approximations for both the wave free-surface deflection (the regular series q_r) and the waves (the exponentially small q_{exp}) could be developed using the method of steepest descents. We now address how this optimally truncated result relates to the Tulin (1983), Tuck (1990, 1991*a*,*b*), and other simplifications discussed in § 2.3.

https://doi.org/10.1017/jfm.2016.818 Published online by Cambridge University Press

9.1. *Truncation at other values of N*

The result of the Hankel integration, in (8.19), which depends on the late-terms behaviour of the ansatz (4.2), was derived on the assumption that truncation of the regular series expansion occurs at optimal truncation with $N \to \infty$ as $\epsilon \to 0$. In practice, however, it may be useful to develop reduced models that truncate at pragmatic values of N (i.e. one or two); let us discuss what loss in accuracy results from this.

As we have shown, the surface speed is expressed as

$$q(\phi) \sim \left[q_0(\phi) + \epsilon q_1(\phi) + \cdots + \epsilon^{N-1} q_{N-1}(\phi)\right] + \left[\mathcal{A}F(\phi)\mathrm{e}^{-\chi(\phi)/\epsilon} + \text{c.c.}\right], \tag{9.1}$$

where we have written the exponential (8.18) in a form so as to separate a numerical prefactor, $\mathcal{A}$, from the functional dependence, $F(\phi)$.

The case of truncation at $N = 1$ is asymptotically inconsistent since, if $q = q_0 + \bar{q}$, then $\bar{q}$ contains both an $O(\epsilon)$ error and also the exponentially small waves we desire. But from (7.2*a*) and (7.2*c*), we see that it would then be incorrect to ignore $O(\bar{q}^2)$ errors in deriving the linearized equation. Despite these issues it is still instructive to examine the truncation at $N = 1$. This yields

$$\epsilon\bar{q}' + \chi'\bar{q} \sim -\epsilon q_0', \tag{9.2}$$

and the solution

$$\bar{q} \sim -\left[\int_{w_s}^{w} q_0' \mathrm{e}^{\chi/\epsilon}\ \mathrm{d}t\right] \mathrm{e}^{-\chi/\epsilon}, \tag{9.3}$$

for an initial point of integration, $t = w_s$, where $\bar{q}(w_s) \to 0$.

Thus the exponential argument, $\mathrm{e}^{-\chi/\epsilon}$, of the solution can be derived from (9.2), and indeed the steepest descent paths of § 8 are still applicable. However we have inaccurately predicted the functional dependence, $F(\phi)$.

The case of truncation at $N = 2$ is much more interesting. It yields

$$\epsilon\bar{q}' + \left[\chi'(w) + \epsilon P_1'(w)\right]\bar{q} \sim -\epsilon^2\left(-\frac{5\mathrm{i}jq_1^2}{2q_0^4} + q_1' + 2\mathrm{i}\frac{\hat{\mathscr{H}}[\theta_1]q_1}{q_0^3}\right). \tag{9.4}$$

Thus, comparing (9.4) to (7.2), we have obtained the precise left-hand side required. In developing the leading-order exponential, the only error in (9.4) is due to the replacement of the exact right-hand side by its $N = 2$ truncation. This only affects the integrand of (8.4), whose role was to determine the prefactor $\mathcal{A}$. In other words, the linear equation (9.4) allows us to develop nearly all of the leading-order exponential. We will see in the numerical computations that this equation provides a very close fit to results from the full nonlinear model. The two-term truncation is the closest analogy to the Tulin (1983) model (see § 10 for an extended discussion), as well as various other models (cf. the review by Doctors & Dagan 1980). However the fact that such two-term approximations do not accurately predict the prefactor $\mathcal{A}$ is not well established in the literature.

9.2. *A simplified nonlinear model for N = 2*

An even simpler formulation to (9.4) can be developed at the risk of slightly increased inaccuracy. This form serves as an extremely useful toy model due to the complete removal of the Hilbert transform, and thus in this sense, it provides the strongest

https://doi.org/10.1017/jfm.2016.818 Published online by Cambridge University Press

analogy to the Tuck reduction of (2.6). Let us return to combined integro-differential equation in (5.8). Approximating $\mathrm{e}^{j\hat{\mathscr{H}}[\theta]} \sim 1$, we obtain

$$\epsilon q' + \frac{\mathrm{i}j}{2}\frac{1}{q_s q^3}\left[q^2 - q_s^2\right] = 0. \tag{9.5}$$

In order to avoid confusion, we shall write the solution of (9.5) as $\tilde{q}$. Expressing $\tilde{q}$ as a regular series expansion $\tilde{q} = \tilde{q}_0 + \epsilon\tilde{q}_1 + \cdots$, we find

$$\tilde{q}_0 = q_s \quad \text{and} \quad \tilde{q}_1 = \mathrm{i}j\tilde{q}_0^3\tilde{q}_0'. \tag{9.6a,b}$$

The leading-order solution is as expected, but ignoring the $\hat{\mathscr{H}}[\theta]$ complex Hilbert transform has the effect of changing the correction term, $\tilde{q}_1$. If we return to the correct q_1 in (4.1*c*), we find that

$$q_1 = jq_0\mathscr{H}[\theta_1] = jq_0(\hat{\mathscr{H}}[\theta_1] - \mathrm{i}\theta_1) = \mathrm{i}jq_0^3q_0' + jq_0\hat{\mathscr{H}}[\theta_1] \tag{9.7}$$

upon using (5.3) and the solution for θ_1 in (4.1*d*). Recall that near the wave-generating singularity, $\hat{\mathscr{H}}[\theta_1]$ remains bounded, but q_0 and its derivatives are singular according to (8.10). In other words, the simplified formulation of (9.5) has replaced q_1 in the full model with its local behaviour near the singularity.

Substituting $q = \tilde{q}_0 + \epsilon\tilde{q}_1 + \cdots + \bar{q}$ into the simplified nonlinear model (9.5) and linearizing in $\bar{q}$ yields

$$\epsilon\bar{q}' + \left[\chi' + \epsilon\frac{5q_0'}{q_0}\right]\bar{q} \sim \tilde{R}(w), \tag{9.8}$$

where we have withheld the right-hand side, $\tilde{R}$, for clarity. From (8.2) and (9.7), we can verify that as $w \to w_0$, $P_1' \sim 5q_0'/q_0$. Comparing the bracketed terms in (9.4) and (9.8), we thus see that in the simplified model, the $\hat{\mathscr{H}}[\theta]$ terms are neglected but we have nevertheless preserved the inner limit of (9.4). Since the Hankel contour analysis of § 8.4 depends only on local properties near the relevant singularities, we conclude that the salient details of the water wave analysis are still largely preserved for the model in (9.5). Consequently, as it concerns the resultant waves, the model is not able to duplicate the exact functional form of the prefactor, but does produce a prefactor that contains the correct inner limit.

In the study of Trinh & Chapman (2015), this simplified nonlinear problem was used as a toy model for the study of wave–structure interactions with coalescing singularities. By duplicating the derivation of § 8, the analogous formula to (8.20) can be developed for (9.5).

A detailed summary of the full and simplified models we have presented thus far is shown in table 2.

9.3. *Numerical results of the stern-flow problem*

We now compare numerical solutions of three reduced models with the full nonlinear stern-wave problem in the limit $\epsilon \to 0$. The models include (i) the full nonlinear problem (5.8), or more conventionally, the solution of Bernoulli's equation (2.1) and the boundary integral equation (3.6); (ii) the $N = 2$ truncated linear model in (9.4); and (iii) the $N = 2^*$ nonlinear model in (9.5).

https://doi.org/10.1017/jfm.2016.818 Published online by Cambridge University Press

https://doi.org/10.1017/jfm.2016.818 Published online by Cambridge University Press

Truncation	Equation	χ	$F(\phi)$	$\mathcal{A}$	Notes
None	$\epsilon q' + \mathrm{i}j/(2q_s q^3)(q^2 \mathrm{e}^{-j\mathscr{H}[\theta]} - q_s^2 \mathrm{e}^{j\mathscr{H}[\theta]}) = 0$	yes	yes	yes	The full nonlinear problem (5.8) requires solving a non-local integro-differential formulation. Real and complex parts yield equations for q and θ.
None	$\epsilon(G'/G) - (\mathrm{i}j/G) + \mathcal{P}(w, q, \theta) = -\mathcal{Q}(w, q, \theta)$	yes	yes	yes	Tulin's formulation (6.1), in terms of $G = (q\mathrm{e}^{-\mathrm{i}j\theta})^3$, is difficult to use due to unknown $\mathcal{Q}$. Note that nonlinear $\mathcal{P}$, with $\mathrm{Re}(\mathcal{P}) = 4\sin^3\theta/q^3$ cannot be written in terms of G, and neglecting $\mathcal{P}$ is equivalent to a truncation at $N = 2$.
$N = 1$	$\epsilon\bar{q}' + \chi'\bar{q} = O(\epsilon)$	yes	no	no	From (9.2); despite simplicity, contains many key properties of the water waves; one-term truncation used in Ogilvie (1968).
$N = 2$	$\epsilon\bar{q}' + (\chi' + \epsilon P_1')\bar{q} = O(\epsilon^2)$	yes	yes	no	From (9.4); the simplest model that preserves everything but the prefactor $\mathcal{A}$. Provides a very close fit to the full nonlinear solutions.
$N = 2^*$	$\epsilon q' + \mathrm{i}j/(2q_s q^3)(q^2 - q_s^2) = 0$	yes	no*	no	From (9.5); simplified nonlinear model that uses inner limit to replace the Hilbert transform; used as toy model in Trinh & Chapman (2015).
$N \to \infty$	$\epsilon\bar{q}' + (\chi' + \epsilon P_1')\bar{q} = O(\epsilon^N)$	yes	yes	yes	From (7.2*a*) with (8.13); the correct linearized equation that preserves all aspects of the leading-order exponential; requires optimal truncation and numerical computation of the prefactor $\mathcal{A}$.

TABLE 2. A comparison of different truncated models for the study of gravity waves past moving bodies, and their ability to correctly predict (yes/no) the leading-order exponential, $\mathcal{A}F(\phi)\mathrm{e}^{-\chi/\epsilon}$ (to be added to its complex conjugate on the free surface). The case of $N = 2^*$ is a two-term truncation that extracts the singular behaviour of the Hilbert transform, and thus obtains the correct functional form of $F(\phi)$ near the relevant singularity, $w = w_0$.

We study the case of a semi-infinite rectangular ship given by (3.11) and (3.12) with $\sigma = 1/2$, and thus

$$q_0 = \left(\frac{w}{w+1}\right)^{1/2}, \tag{9.9}$$

which is the leading-order speed associated with a hull with a right-angled corner ($3\pi/2$ in the interior of the fluid) at $w = -1$, and a stagnation point at $w = 0$.

The solution is computed in each of the three cases, and the amplitude of the water waves far downstream, with $w = \phi \gg 1$, is extracted. For the two models with truncations at $N = 2$ and $N = 2^*$, recall that the real-valued solution on the axis is formed by adding the complex-valued solution to its complex conjugate [see (8.19) and the surrounding discussion]. Thus, for these two cases, the amplitude of q is taken to be twice the amplitude of $\mathrm{Re}(q_{exp})$.

In order to solve the full water-wave equations (5.8), we use the numerical algorithm described in Trinh *et al.* (2011). In brief, a stretched grid is applied near the stagnation point, and a finite-difference approximation of the boundary integral is calculated using the trapezoid rule. At a singular point of the integral, a quadratic interpolant is applied between the point and its two neighbours, and the resultant quadratic is calculated exactly. For more details of the numerical scheme see, e.g. Chapter 7 of Vanden-Broeck (2010) and the references therein. From the predicted wave amplitude (8.20), we have

$$\text{Amplitude of } q_{exp} = \left[\frac{\tilde{C}}{\epsilon^{\gamma}}\right] \mathrm{e}^{-3\pi/(2\epsilon)}, \tag{9.10}$$

where $\tilde{C} \approx 2.215$, $\gamma = 6\sigma/(1+3\sigma)$, and here, $\sigma = 1/2$. The numerical prefactor $\tilde{C}$ requires a generic calculation (cf. figure 10 of Trinh *et al.* 2011). Both numerical amplitude measurements (stars), as well as the asymptotic prediction (upper dashed line), are shown in figure 5.

The $N = 2$ and $N = 2^*$ truncated models can be solved as initial value problems. Due to the singular nature of the stagnation point, where $q = O(w^{1/2})$, we use the coordinate transformation $s(w) = w^{1/2}$, and solve the associated differential equations in s. The asymptotic behaviour (9.9) is used to provide the initial value for q at a point near $s = 0$. In the simulations, we typically used $s = 10^{-5}$ for this point, and the resultant amplitudes are verified to be independent of the initial condition.

The combined results are shown in figure 5. The leading-order asymptotic approximations fit the data closely, and both the simplified nonlinear ($N = 2^*$, shown as circle) and linear ($N = 2$, shown as stars) formulations duplicate the requisite behaviours reviewed in table 2. Note that although the emphasis of this work is largely on the development of the mathematical framework, the numerical results indicate that the low-speed theory is able to predict both the exponential dependence to some of the typical values of the Froude number in ship hydrodynamical applications (see Wehausen (1973) for more details).

9.4. *Numerical results of the step-wave problem*

Numerical solutions for flow past a step of angle $\pi\sigma$ are computed by solving the coupled system of (2.1) and (3.6), but now with the adjusted map (3.4) and leading-order speed (3.10). Description of the numerical scheme and asymptotic comparisons with the optimally truncated model have been presented in Chapman

https://doi.org/10.1017/jfm.2016.818 Published online by Cambridge University Press

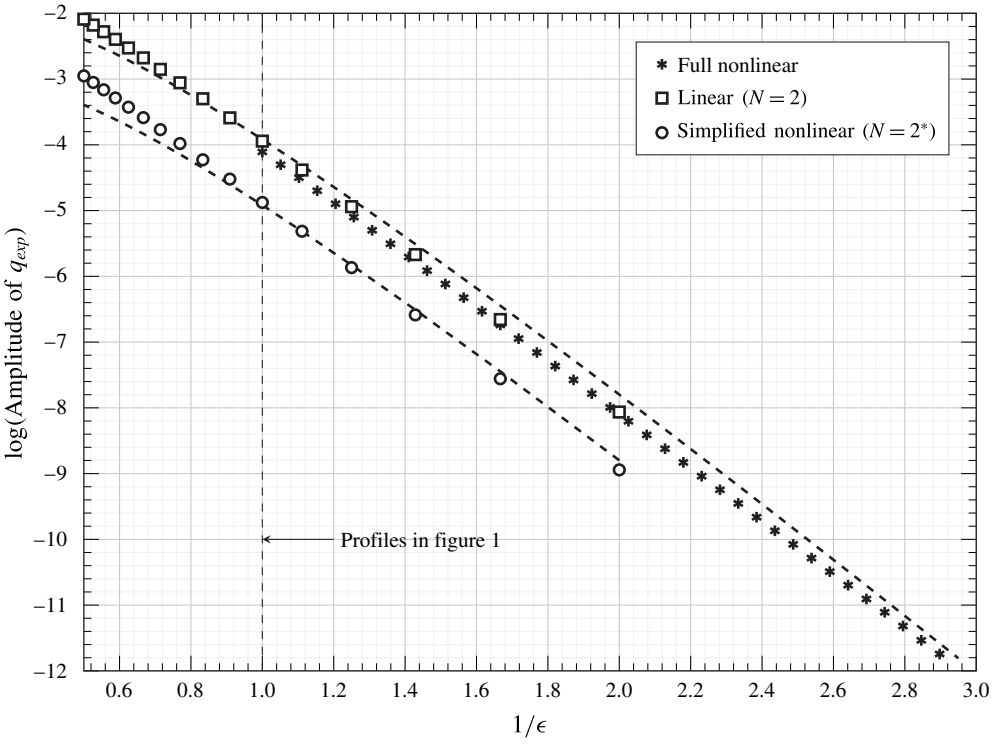


FIGURE 5. Comparison of wave amplitudes for the full nonlinear model, the $N = 2$ truncated linear model, and the $N = 2^*$ truncated nonlinear model. For the two truncated models, the amplitude is multiplied by two to account for the analytic continuation. The dashed lines correspond to leading-order asymptotic approximations of the full nonlinear model (top) and the simplified nonlinear model (bottom).

& Vanden-Broeck (2006, figures 5–8) and Lustri *et al.* (2012, figures 4, 9). In this section, we provide some additional discussion of the Stokes line structure, and how it relates to the formation of waves.

A typical solution is shown in figure 6(*a*) for the case of a rectangular step with $\sigma = 1/2$ at $\epsilon = 0.35$. Note the sharpened crests and wide troughs of the surface waves; we have chosen the Froude number to be particularly large in order to better visualize the free surface. In order to plot streamlines in the physical plane, we calculate values of the complex velocity, $qe^{-i\theta}$, in the lower half-ζ-plane using the analytic continuation of the boundary integral (5.5) with $j = -1$ and $k = -1$. Once q and θ are known, the physical x and y-coordinates along streamlines follow from integrating (3.2).

In § 8.2, we showed that for a given flow problem, Stokes lines within the integration plane of (8.4*b*) are associated with sudden changes in the steepest descent paths. Across such lines, waves are switched-on via a Hankel contour around a particular singularity (cf. § 8.4). We also noted in § 5.1 that, although Stokes lines lie in a non-physical region of space (the analytic continuation of the free surface), they can often be projected into physical space. In the case of the rectangular step of figure 6(*a*), we do this computation as follows.

First, a separate analysis indicates that the stagnation point of the step does not produce a Stokes line (Chapman & Vanden-Broeck 2006). Thus, the initial point of

https://doi.org/10.1017/jfm.2016.818 Published online by Cambridge University Press

https://doi.org/10.1017/jfm.2016.818 Published online by Cambridge University Press

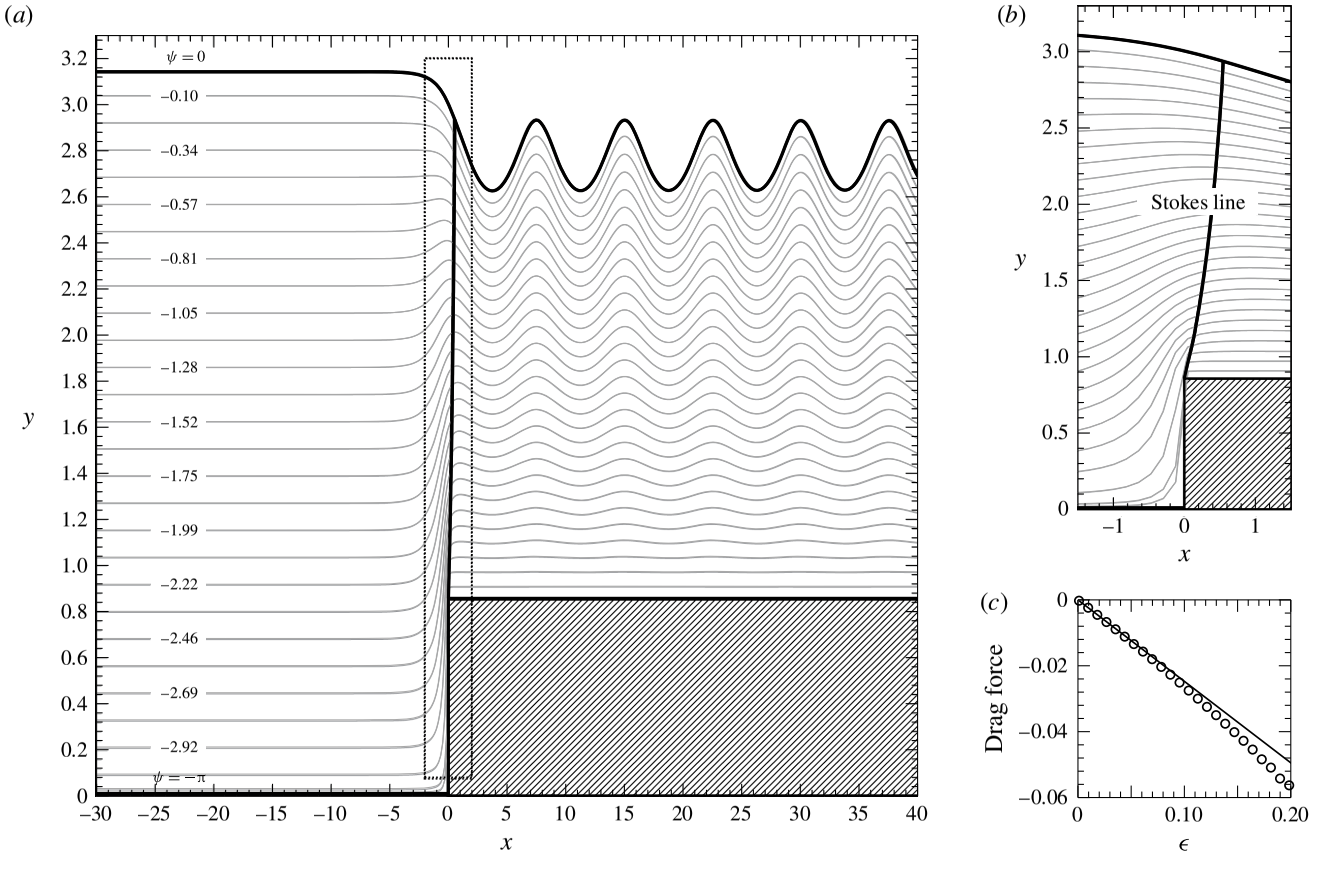


FIGURE 6. (*a*) Flow past the rectangular step defined by (3.10) with $\sigma = 1/2$, $a = 1$ and $b = 2.2$. The solution is computed using the full nonlinear equations (2.1) and (3.6) at $\epsilon = 0.35$. Streamlines are calculated by analytic continuation of the boundary integral into the fluid region. Also shown is the projection of the Stokes line, where $\mathrm{Im}\,\chi = 0$ and $\mathrm{Re}\,\chi \geqslant 0$, which emerges from the corner, $\zeta = -a$ or $(x, y) \approx (0, 0.86)$. An enlargement of the region near the Stokes line is shown in (*b*). The drag force on the step is shown in (*c*) and computed from (9.11) for different ϵ. As $\epsilon \to 0$, the drag behaves as $D = -\pi\epsilon(\sqrt{a} - \sqrt{b})^2/\sqrt{4ab} + O(\epsilon^2)$.

integration of χ in (8.1) is chosen at the corner of the step, $\zeta = -a$ or $w_0 = -\log|a| - \pi\mathrm{i}$. The Stokes line then consists of points where $\{\mathrm{Im}\,\chi = 0, \mathrm{Re}\chi \geqslant 0\}$, and this is computed by numerical quadrature in the ζ-plane. Once the Stokes line is known in the ζ-plane or equivalently the w-plane, it can be projected into the (x, y)-plane by interpolation of the streamlines of the flow. The result is shown in figure 6(*a*) and a close-up in figure 6(*b*). The Stokes line marks the location in the flow where the waves switch on following the rise in the step. At finite values of ϵ, the transition occurs in a boundary layer of appreciable thickness (Berry 1989).

There are several interesting consequences of considering the low-speed limit of $\epsilon \to 0$ and viewing the Stokes line projected into the physical plane. For example, King & Bloor (1987) had considered the non-dimensional drag force on the face of the step given by,

$$D = \frac{\epsilon}{2}\int_{y=0}^{y=h} [1 - q^2]\,\mathrm{d}y = \frac{\epsilon}{2}\int_{\zeta=-b}^{\zeta=-a} [1 - q^2]\left[-\frac{\sin(\pi\sigma)}{q\zeta}\right]\mathrm{d}\zeta, \tag{9.11}$$

where h is the step height in the physical plane. In the limit $\epsilon \to 0$, the drag can be approximated by integrating (9.11) with the speed given by the leading-order speed, q_0, and this is verified in figure 6(*c*). The higher-order terms, q_1, q_2, and so forth produce further algebraic corrections of the drag force. In the case of general angled steps, waves may be switched on in the region between $\zeta = -b$ and $\zeta = -a$, and therefore, the wave field may affect the drag force to an exponentially small degree (cf. Stokes line diagrams in Lustri *et al.* (2012) and Trinh (2016)).

10. Discussion

Throughout our analysis of §§ 7–9, we have chosen to stray from Tulin's formulation, which is encapsulated in the study of (1.1). This mode of presentation was out of necessity; while the broad outline of Tulin's reduction is ultimately correct, the use of the unknown $\mathcal{Q}$-function renders the equation impractical for most applications. Moreover, the Davies (1951) substitution (2.2) and subsequent truncation of the nonlinear $\mathcal{P}$ does not make clear what inaccuracies are introduced by the reduction process (we have concluded, for example, that the prefactor of the wave will be incorrect). We have provided an extended discussion of Tulin's $\mathcal{Q}$-function in appendix B, and the connections with our own formulation in § 6 and appendix C.

While Tulin's work may have been unappreciated since its inception, the work was, in fact, ahead of its time. Indeed, the proposal of the complex-variable reduction of the water-wave equations, and the subsequent simplification of the Hilbert transform would anticipate many of the more sophisticated asymptotic approaches that would later develop independently (e.g. in Chapman & Vanden-Broeck 2006). As we have reviewed in § 2.3, others have proposed integral formulations of the low-Froude-number problem (see e.g. the collection of models in Doctors & Dagan 1980), but such models typically depended on ad-hoc linearizations of the two-dimensional potential flow equations.

Also at the forefront of our motivation was to better understand Tuck's series of papers (Tuck 1990, 1991*a*,*b*), which had posited simplified toy models that could eliminate the Hilbert transform while preserving essential details of the waves. During the brief exchange between Tulin and Tuck, as quoted in § 1.2, Tuck had indicated that it was unclear whether his reductions were related, via the complex plane, with Tulin's model. The answer is that they are indeed related.

https://doi.org/10.1017/jfm.2016.818 Published online by Cambridge University Press

Through our corrected reduction (7.2) and the subsequent study using the method of steepest descents, we were able to explain why the Hilbert transform is crucial in some cases (determining $I_{endpoints}$), but may be negligible in others (determining I_{exp}). This idea of being able to study and visualize wave–structure interactions using the method of steepest descents is a powerful one, and we believe that it has wider applicability to the study of flows with more complicated geometries.

10.1. *Which model is correct?*

Another main result of our work relates to the presentation of table 2, which unifies the various truncated models under consideration. We have shown that in the limit $\epsilon \to 0$, the exponentially small water waves are of the form $\mathcal{A}F(\phi)\mathrm{e}^{-\chi/\epsilon}$ plus its complex conjugate.

In order to obtain the correct χ, we can solve the one-term truncated model

$$\epsilon\bar{q}' + \chi'(w)\bar{q} \sim -\epsilon q_0'. \tag{10.1}$$

This is the simplest reduction of the water-wave problem. Despite the fact that it incorrectly predicts $\mathcal{A}F(\phi)$, it still serves as a useful toy model since the steepest descent argument remains unchanged.

If we wish to obtain the correct functional form of $F(\phi)$, then we can instead solve the equation,

$$\epsilon\bar{q}' + \left[\chi'(w) + \epsilon P_1'(w) + O(\epsilon^2)\right]\bar{q} = R(w; \hat{\mathscr{H}}[\bar{\theta}]), \tag{10.2}$$

where R will be truncated to $O(\epsilon^2)$ error, as detailed in table 2.

It is difficult to propose any reduced equation that allows us to determine the correct numerical prefactor, $\mathcal{A}$, since this involves inclusion of terms up to optimal truncation in q_r and θ_r. Since this optimal truncation term tends to infinity as $\epsilon \to 0$, then we must do as we have done in e.g. (8.13), and approximate R using its divergent form. This is the connection with previous approaches that have used exponential asymptotics. The correct model – that is to say, the one that predicts the leading-order exponential up to the numerical prefactor – does indeed require knowledge of how the asymptotic series diverges.

10.2. *Reviewing Tulin's low-speed comments*

Tulin's paradoxical comment regarding the validity of the low-speed limit, quoted in our introduction, will be resolved once the specific problem geometry and integrand functions of (8.4) is considered using the method of steepest descents. To review, Tulin had noted that in the limit $\epsilon \to 0$, there would be locations on the free surface where the waves would grow in an unbounded manner. In the language of our work, this corresponds to the unbounded nature of the wave, $\mathrm{e}^{-\chi/\epsilon}$ at the points where $\chi = 0$.

However, we have seen through the methodology of § 8 that for the case of flow past e.g. a ship or a step, in the limit $\epsilon \to 0$, the waves arise from the submerged corner of the body. It is at this point that $\chi = 0$ and the waves are large (and unbounded if the critical point is approached in certain directions). Otherwise, the waves remain exponentially small everywhere along the free surface, and indeed, it was precisely this argument that had allowed us to neglect the Hilbert transform. Therefore, there is no issue with taking the $\epsilon \to 0$ limit within the physical domain. This is confirmed by the numerical verification of the same limit.

Tulin's comment, however, has an important consequence in the case of bow flows. In this case, we see that as the solution is analytically continued in the direction of

https://doi.org/10.1017/jfm.2016.818 Published online by Cambridge University Press

the bow, the generated exponential, of order $e^{-\chi/\epsilon}$, will tend to infinite amplitude at the stagnation point. Thus there is no bounded solution in the $\epsilon \to 0$ limit for bow flow (Vanden-Broeck & Tuck 1977; Trinh *et al.* 2011).

10.3. *Applicability of reduced models to further studies*

In an age where there are a bevy of tools and packages that can perform full numerical computations of the nonlinear water-wave problem, the reader may be justified in wondering whether there is still applicability in studying the significance of historical works by Tulin (1983), Tuck (1990, 1991*a*,*b*), and this paper itself. As summarized by table 2, the differences between various truncated models are subtle, and given the current state of computation, it seems more difficult to unravel such subtleties than it is to solve the full model.

However, while methods of computation have improved significantly since Tulin's 1983 paper, many theoretical aspects of free-surface wave–body flows are still a mystery, as evidenced by the review in Tulin (2005). For example, there is virtually no analytical theory that can distinguish between waves produced by surface-piercing bodies with sudden angular changes (corners) versus bodies that are smooth (cf. the discussion in Trinh & Chapman (2014)). The classic treatments using linearized theory, as it appears in e.g. Kostyukov (1968) and Wehausen (1973), are limited to asymptotically small bodies rather than the bluff bodies we consider in this paper. Thus the methodology proposed in this paper provides a valuable tool for theoretical analysis of difficult wave–structure problems where the nonlinearity in the geometry can be preserved. In a forthcoming work, we will demonstrate how the steepest descent methodology developed in this paper can be applied to the study of smooth-bodied obstructions.

The techniques and reductions presented in this paper, along with further developments in the theory of exponential asymptotics, provides hope that analytical progress can be made on the subject of time-dependent and three-dimensional wave–body problems (cf. recent work by Howls, Langman & Daalhuis (2004), Chapman & Mortimer (2005), Lustri & Chapman (2014) and Bennett (2015) on this topic).

Acknowledgement

I am grateful for correspondences with Professor M. Tulin, who provided enthusiasm and encouragement for pursuing the problems raised in his 1983 manuscript.

Appendix A. Form of the divergence

The individual components, Q, χ, and γ, that make up the factorial-over-power divergence in (4.2) can be derived by examining the governing equations at $O(\epsilon^n)$. In the limit $n \to \infty$, the leading-order contribution gives the singulant, χ,

$$\frac{\mathrm{d}\chi}{\mathrm{d}w} = \frac{\mathrm{i}jk}{q_0^3}, \tag{A 1}$$

and since $\chi = 0$ at the singularities, we write

$$\chi = \mathrm{i}jk \int_{w_0}^{w} \frac{\mathrm{d}\varphi}{q_0^3(\varphi)}, \tag{A 2}$$

where $w = w_0$ is a particular singularity of the leading-order solution.

https://doi.org/10.1017/jfm.2016.818 Published online by Cambridge University Press

Similarly, it can be shown that

$$Q(w) = \frac{\Lambda}{q_0^2(w)} \exp\left[3\mathrm{i}jk \int_{w^*}^{w} \frac{q_1(\varphi)}{q_0^4(\varphi)}\, \mathrm{d}\varphi\right], \tag{A 3}$$

where Λ is a constant of integration and w^* is an arbitrary point chosen wherever the integral is defined. The prefactor Θ, is then related to Q using

$$Q = (\mathrm{i}jk) q_0 \Theta. \tag{A 4}$$

The value of γ is derived by matching the local behaviour of q_n in (4.2) with leading order q_0 near the singularity, $w = w_0$. If we assume that $q_0 \sim c(w - w_0)^\alpha$ near the singularity, then

$$\gamma = -\frac{6\alpha}{1 - 3\alpha}. \tag{A 5}$$

For most nonlinear problems, the value of Λ in (A 3) embeds the nonlinearity of the governing equations near the singularity, and must be found through a numerical solution of a recurrence relation. A detailed derivation of the above quantities, including numerical values of Λ, can be found in § 3.1 of Chapman & Vanden-Broeck (2006) and § 4 of Trinh *et al.* (2011). We also refer the reader to more general reviews of exponential asymptotics by Olde Daalhuis *et al.* (1995), Boyd (1998) and Costin (2008).

Appendix B. The limitations of the $\mathcal{Q}$-function

The most difficult aspect of Tulin's work concerns Section VI of the manuscript, which seeks to understand the nature of the analytically continued function, $\mathcal{Q}(w)$. We will attempt to follow the same argument as Tulin (with adjustments for changes in notation and flow geometry).

Tulin had split the form of $\mathcal{Q}$ into a contribution from the uniform flow and a contribution from the geometry. In his notation, our $\mathcal{Q}(w)$ is equal to $\mathrm{i}j - Q(w)$ (note this is Tulin's notation and not the Q in the divergent form (A 3)). The situation of an imposed pressure distribution was also considered in his work, but we shall ignore this effect. Tulin had then written $\mathcal{Q}$ in terms of a Cauchy integral over the solid boundary and its image reflected about the free surface in the potential plane. This is analogous to applying Cauchy's integral theorem to either G or the hodograph variable (3.3) along a counterclockwise circular contour of radius $R \to \infty$ with a slit about the negative real axis (see figure 7*b*). This yields

$$\log q(\zeta) - \mathrm{i}\theta(\zeta) = \frac{1}{2\pi\mathrm{i}} \left(\int_{circle} + \int_{slit}\right) \left[\frac{\log q - \mathrm{i}\theta}{t - \zeta}\right] \mathrm{d}t, \tag{B 1}$$

where the integral along the outer circle tends to zero as $R \to \infty$ by the boundary conditions and the integral over the slit involves $q^\pm$ and $\theta^\pm$, the limiting values from the upper or lower half-planes. However, in (B 1), only the values of θ on one side are known (being the physical angle of the solid boundary). For instance, in the case of a step, $\theta^+(t)$ is given by (3.9). The problem, however, is that the other values $\theta^-(t)$, $q^+(t)$, and $q^-(t)$ are only known through analytic continuation, and it is impossible to go further with (B 1) without additional information.

For most practical implementations, it is preferable to instead apply Cauchy's Theorem to an integral over the solid boundary and the free surface (see figure 7*a*),

https://doi.org/10.1017/jfm.2016.818 Published online by Cambridge University Press

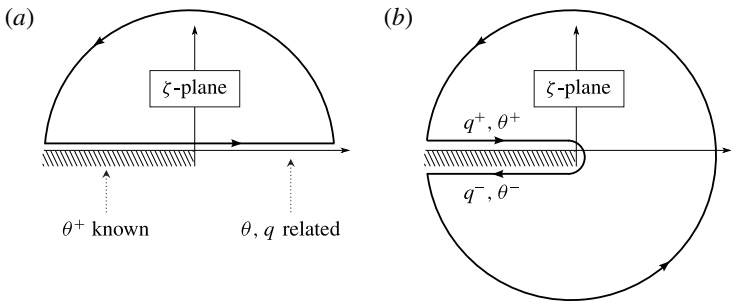


FIGURE 7. (*a*) The Cauchy contour used to derive the boundary integral formulation (3.5); (*b*) the Cauchy contour used in Tulin's $\mathcal{Q}$-function.

which was the formulation in § 3.1. Bernoulli's equation is required in order to provide a relationship between q and θ on the free surface, and thus close the system.

Tulin had posited that the value of $\mathcal{Q}$ might be found through a theoretically posited surrogate body whose singularities on the physical boundary alone would generate the flow (rather than the physical boundary and its reflected image). This appears as equation (60) in his work. However, for a given physical geometry (e.g. for the step and ship geometries of § 3), it is unclear how this surrogate body could ever be determined in an *a priori* fashion.

Thus in the end, Tulin's $\mathcal{Q}(w)$ should rather be written as $\mathcal{Q}(w; q, \theta)$, as it involves the solution itself. This creates a problematic argument if the intention is to treat (1.1) as an ordinary differential equation to be integrated exactly, for the solution appears on both sides of the formulation. Indeed, this is precisely the issue that Tuck (§ 2.2) had wrestled with, in seeking a reduction of the global Hilbert transform operator.

Appendix C. Connection to Tulin's formulation

As explained in § 6, we have chosen to stray from Tulin's formulation, which uses the combined analytic function, $G = (q\mathrm{e}^{-\mathrm{i}j\theta})^3$, and the unknown right-hand side, $\mathcal{Q}$. Our formulation separates the analytic continuations of the q and θ variables, and is self-contained. In contrast, Tulin's formulation requires the specification of the $\mathcal{Q}$-function, which requires additional information. We now wish to show how Tulin's equation (6.1) is related to the equation for the exponential in § 8.4, given by

$$\epsilon\bar{q}' + \left[\chi' + \epsilon P_1'\right]\bar{q} \sim -\epsilon^N q'_{N-1}, \tag{C 1}$$

that is, the reduced integro-differential model (7.2*a*) with the right-hand side (8.13).

In order to relate the two formulations, we multiply (6.1) through by G and obtain

$$\epsilon\frac{\mathrm{d}G}{\mathrm{d}w} - \mathrm{i}j + (\mathcal{P}G) = -\mathcal{Q}G. \tag{C 2}$$

We expand the unknown functions in the above equation into a regular perturbation expansion and an error term, using

$$G = G_r + \bar{G}, \quad (\mathcal{P}G) = (\mathcal{P}G)_r + \overline{\mathcal{P}G}, \quad \mathcal{Q} = \mathcal{Q}_r + \bar{\mathcal{Q}}, \tag{C 3a–c}$$

https://doi.org/10.1017/jfm.2016.818 Published online by Cambridge University Press

where for simplicity, we expand the product $(\mathcal{P}G)$ rather than the individual factors. Substitution into (C 2) gives

$$\epsilon\frac{\mathrm{d}\bar{G}}{\mathrm{d}w}+\mathcal{Q}_r\bar{G}=-\hat{\mathcal{E}}_{bern}+O(\bar{\mathcal{Q}},\overline{\mathcal{P}G}), \tag{C 4}$$

where we have introduced the error in the Bernoulli equation,

$$\hat{\mathcal{E}}_{bern}=\epsilon\frac{\mathrm{d}G_r}{\mathrm{d}w}-\mathrm{i}j+(\mathcal{P}G)_r+\mathcal{Q}_rG_r, \tag{C 5}$$

which can be compared to (7.2*e*). The expansion of $G=(G_0+\epsilon G_1+\cdots)+\bar{G}$, can also be written in terms of the expansions for q and θ. Using $G=(q\mathrm{e}^{-\mathrm{i}j\theta})^3$, and expanding, we find

$$G_0=q_0^3,\quad G_1=3q_0^2q_1-3\mathrm{i}jq_0^3\theta_1, \tag{C 6a,b}$$

$$\bar{G}=\left[3q_0^2\bar{q}-3\mathrm{i}jq_0^3\bar{\theta}\right]+\epsilon\left[-9\mathrm{i}jq_0^2q_1\bar{\theta}-9\mathrm{i}jq_0^2\theta_1\bar{q}+6q_0q_1\bar{q}-9q_0^3\theta_1\bar{\theta}\right]+\cdots. \tag{C 6c}$$

Following the discussion in § 6 and appendix B, we emphasize that q_0, q_1, θ_1, and the low-order terms are derived independently from (C 2) – that is, the single equation for G is insufficient to close the system without inclusion of the Hilbert transform. Instead, we assume that the low-order terms in (C 6) are known and that (C 2) provides an equation for $\mathcal{Q}$. The regular part of $\mathcal{Q}$, given by $\mathcal{Q}_r$, follows from expansion of the left-hand side of (6.1). Only including up to $O(\epsilon^2)$ terms, we obtain

$$-\mathcal{Q}_r=\epsilon\frac{G_0'}{G_0}-\frac{\mathrm{i}j}{G_0}+\epsilon\frac{\mathrm{i}jG_1}{G_0^2}+O(\epsilon^2)=-\frac{\mathrm{i}j}{q_0^3}-\epsilon\left[-\frac{3q_0'}{q_0}-\frac{3\theta_1}{q_0^3}-\frac{3\mathrm{i}jq_1}{q_0^4}\right]+O(\epsilon^2). \tag{C 7}$$

We also note that in the limit $\epsilon\to 0$, the optimal truncation point of the regular series expansion tends to infinity, $N\to\infty$, and the error in Bernoulli's equation is replaced by the divergent term

$$\hat{\mathcal{E}}_{bern}\sim\epsilon^NG_{N-1}', \tag{C 8}$$

which is analogous to the argument leading to (8.13). The result now follows by using (4.1*c*,*d*) for q_1 and θ_1, (C 6*c*) for $\bar{G}$, (C 7) for $\mathcal{Q}_r$, and (C 8) for the right-hand side of (C 4). We are left with

$$\epsilon\bar{q}'+\left[\frac{\mathrm{i}j}{q_0^3}+\epsilon\left(\frac{2q_0'}{q_0}-\frac{3\mathrm{i}jq_1}{q_0^4}\right)\right]\bar{q}\sim-\epsilon^Nq_{N-1}', \tag{C 9}$$

or (C 1), as desired. Thus we have shown how Tulin's formulation will exactly preserve the exponentially small surface waves. Derivation of the full relationship of Tulin's equation to the full system (7.2) can be similarly done, but the algebra (in expanding $\mathcal{Q}$ and G, and returning to the formulation with the embedded Hilbert transform) becomes unwieldy.

REFERENCES

BENNETT, T. 2015 Exponential asymptotics for integrals with degenerate and non-isolated critical points. PhD thesis, University of Southampton.

https://doi.org/10.1017/jfm.2016.818 Published online by Cambridge University Press

BERRY, M. 1991 Asymptotics, superasymptotics, hyperasymptotics. In *Asymptotics Beyond All Orders* (ed. H. Segur), pp. 1–14. Springer.

BERRY, M. V. 1989 Stokes' phenomenon; smoothing a Victorian discontinuity. *Publ. Math. Inst. Hautes Études Sci.* **68**, 211–221.

BLEISTEIN, N. & HANDELSMAN, R. A. 1975 *Asymptotic Expansions of Integrals*. Courier Dover Publications.

BOYD, J. P. 1998 *Weakly Nonlocal Solitary Waves and Beyond-all-orders Asymptotics*. Kluwer Academic Publishers.

BRANDSMA, F. J. & HERMANS, A. J. 1985 A quasi-linear free surface condition in slow ship theory. *Schiffstechnik Bd.* **32**, 25–41.

CHAPMAN, S. J., KING, J. R. & ADAMS, K. L. 1998 Exponential asymptotics and Stokes lines in nonlinear ordinary differential equations. *Proc. R. Soc. Lond.* A **454**, 2733–2755.

CHAPMAN, S. J. & MORTIMER, D. B. 2005 Exponential asymptotics and Stokes lines in a partial differential equation. *Proc. R. Soc. Lond.* A **461** (2060), 2385–2421.

CHAPMAN, S. J. & VANDEN-BROECK, J.-M. 2002 Exponential asymptotics and capillary waves. *SIAM J. Appl. Maths* **62** (6), 1872–1898.

CHAPMAN, S. J. & VANDEN-BROECK, J.-M. 2006 Exponential asymptotics and gravity waves. *J. Fluid Mech.* **567**, 299–326.

COSTIN, O. 2008 *Asymptotics and Borel Summability*, vol. 141. Chapman & Hall/CRC.

CRAIG, W. & STERNBERG, P. 1992 Symmetry of free-surface flows. *Arch. Rat. Mech. Anal.* **118** (1), 1–36.

CREW, S. C. & TRINH, P. H. 2016 New singularities for Stokes waves. *J. Fluid Mech.* **798**, 256–283.

DAGAN, G. & TULIN, M. P. 1972 Two-dimensional free-surface gravity flow past blunt bodies. *J. Fluid Mech.* **51** (3), 529–543.

DAVIES, T. V. 1951 The theory of symmetrical gravity waves of finite amplitude. I. *Proc. R. Soc. Lond.* A **208** (1095), 475–486.

DAWSON, C. W. 1977 A practical computer method for solving ship-wave problems. In *2nd International Conference of Numerical Ship Hydrodynamics, Berkeley, USA*. University of California.

DOCTORS, L. J. & DAGAN, G. 1980 Comparison of nonlinear wave-resistance theories for a two-dimensional pressure distribution. *J. Fluid Mech.* **98** (03), 647–672.

FARROW, D. E. & TUCK, E. O. 1995 Further studies of stern wavemaking. *J. Austral. Math. Soc.* B **36**, 424–437.

HOWLS, C. J., LANGMAN, P. J. & DAALHUIS, A. B. OLDE 2004 On the higher-order Stokes phenomenon. *Proc. R. Soc. Lond.* A **460**, 2285–2303.

INUI, T. & KAJITANI, H. 1977 A study on local non-linear free surface effects in ship waves and wave resistance. *Schiffstechnik* **24**, 178–213.

KELLER, J. B. 1979 The ray theory of ship waves and the class of streamlined ships. *J. Fluid Mech.* **91**, 465–487.

KING, A. C. & BLOOR, M. I. G. 1987 Free-surface flow over a step. *J. Fluid Mech.* **182**, 193–208.

KOSTYUKOV, A. A. 1968 *Theory of Ship Waves and Wave Resistance*. Effective Communications Inc.

LUSTRI, C. J. & CHAPMAN, S. J. 2014 Unsteady flow over a submerged source with low Froude number. *Eur. J. Appl. Maths* **25** (05), 655–680.

LUSTRI, C. J., MCCUE, S. W. & BINDER, B. J. 2012 Free surface flow past topography: a beyond-all-orders approach. *Eur. J. Appl. Maths* **1** (1), 1–27.

LUSTRI, C. J., MCCUE, S. W. & CHAPMAN, S. J. 2013 Exponential asymptotics of free surface flow due to a line source. *IMA J. Appl. Maths* **78** (4), 697–713.

MADURASINGHE, M. A. D. & TUCK, E. O. 1986 Ship bows with continuous and splashless flow attachment. *J. Austral. Math. Soc.* B **27**, 442–452.

MILOH, T. & DAGAN, G. 1985 A study of nonlinear wave resistance using integral equations in Fourier space. *J. Fluid Mech.* **159**, 433–458.

OGILVIE, T. F. 1968 Wave resistance: the low speed limit. *Tech. Rep.* Michigan University, Ann Arbor.

https://doi.org/10.1017/jfm.2016.818 Published online by Cambridge University Press

OGILVIE, T. F. & CHEN, S.-X. 1982 Water waves generated by a slowly moving two-dimensional body. Part 1. *Tech. Rep.* DTIC Document.

OLDE DAALHUIS, A. B., CHAPMAN, S. J., KING, J. R., OCKENDON, J. R. & TEW, R. H. 1995 Stokes Phenomenon and matched asymptotic expansions. *SIAM J. Appl. Maths* **55** (6), 1469–1483.

TRINH, P. H. 2010 Exponential asymptotics and Stokes line smoothing for generalized solitary waves. In *Asymptotic Methods in Fluid Mechanics: Survey and Recent Advances* (ed. H. Steinrück), pp. 121–126. Springer.

TRINH, P. H. 2016 A topological study of gravity waves generated by moving bodies using the method of steepest descents. *Proc. R. Soc. Lond.* A **472**, 20150833.

TRINH, P. H. & CHAPMAN, S. J. 2013*a* New gravity-capillary waves at low speeds. Part 1. Linear theory. *J. Fluid Mech.* **724**, 367–391.

TRINH, P. H. & CHAPMAN, S. J. 2013*b* New gravity-capillary waves at low speeds. Part 2. Nonlinear theory. *J. Fluid Mech.* **724**, 392–424.

TRINH, P. H. & CHAPMAN, S. J. 2014 The wake of a two-dimensional ship in the low-speed limit: results for multi-cornered hulls. *J. Fluid Mech.* **741**, 492–513.

TRINH, P. H. & CHAPMAN, S. J. 2015 Exponential asymptotics and problems with coalescing singularities. *Nonlinearity* **28** (5), 1229–1256.

TRINH, P. H., CHAPMAN, S. J. & VANDEN-BROECK, J.-M. 2011 Do waveless ships exist? Results for single-cornered hulls. *J. Fluid Mech.* **685**, 413–439.

TUCK, E. O. 1990 Water non-waves. In *Mini-conference on Free and Moving Boundary and Diffusion Problems, Proceedings of the Centre for Mathematics and its Applications*, pp. 109–127. Centre for Mathematics and its Applications, Australian National University.

TUCK, E. O. 1991*a* Ship-hydrodynamic free-surface problems without waves. *J. Ship Res.* **35** (4), 277–287.

TUCK, E. O. 1991*b* Waveless solutions of wave equations. In *Proceedings of the 6th International Workshop on Water Waves and Floating Bodies*. MIT.

TULIN, M. P. 1983 An exact theory of gravity wave generation by moving bodies, its approximation and its implications. In *Proceedings of the 14th Symposium on Naval Hydrodynamics, Ann Arbor, Michigan*, pp. 19–51. National Academy Press.

TULIN, M. P. 1984 Surface waves from the ray point of view. In *Proceedings of the 14th Symposium on Naval Hydrodynamics*, pp. 9–19. National Academy Press.

TULIN, M. P. 2005 Reminiscences and reflections: ship waves. *J. Ship Res.* **49** (4), 238–246.

VANDEN-BROECK, J.-M. 2010 *Gravity-Capillary Free-Surface Flows*. Cambridge University Press.

VANDEN-BROECK, J.-M. & MILOH, T. 1995 Computations of steep gravity waves by a refinement of Davies–Tulin's approximation. *SIAM J. Appl. Maths* **55** (4), 892–903.

VANDEN-BROECK, J.-M., SCHWARTZ, L. W. & TUCK, E. O. 1978 Divergent low-Froude-number series expansion of nonlinear free-surface flow problems. *Proc. R. Soc. Lond.* A **361**, 207–224.

VANDEN-BROECK, J.-M. & TUCK, E. O. 1977 Computation of near-bow or stern flows using series expansion in the Froude number. In *2nd International Conference on Numerical Ship Hydrodynamics*. University of California.

WEHAUSEN, J. V. 1973 The wave resistance of ships. *Adv. Appl. Mech.* **13**, 93–245.

https://doi.org/10.1017/jfm.2016.818 Published online by Cambridge University Press